



# Design of experiments in the optimization of all-cellulose composites

Ashley Victoria · Peter John Hine · Keeran Ward · Michael Edward Ries

Received: 14 February 2023 / Accepted: 28 September 2023  
© The Author(s) 2023

**Abstract** In this work, statistical design of experiments (DoE) was applied to the optimization of all cellulose composites (ACCs) using cotton textile and interleaf films under applied heat and pressure. The effects of dissolution temperature, pressure and time on ACC mechanical properties were explored through a full factorial design ( $2^3$ ) and later optimized using Response Surface Methodology. It was found that the experimental design was effective at revealing the underlying relationship between Young's modulus and processing conditions, identifying optimum temperature and time settings of 101 °C and 96.8 min respectively, to yield a predicted Young's modulus of 3.3 GPa. This was subsequently validated through the preparation of in-lab test samples which were found to exhibit a very similar Young's modulus of  $3.4 \pm 0.2$  GPa, confirming the adequacy of the predictive model. Additionally, the optimized samples had an average tensile strength and peel strength of  $72 \pm 2$  MPa and  $811 \pm 160$  N/m respectively, as well

as a favorable density resulting from excellent consolidation within the material microstructure. This work highlights the potential of DoE for future ACC process understanding and optimization, helping to bring ACCs to the marketplace as feasible material alternatives.

**Keywords** All cellulose composite · Cellulose textile · Design of experiment · Partial dissolution · Ionic liquid

## Introduction

There has been a surge of interest in recent years in the field of all-cellulose composites (ACCs) and their potential to replace those made from petroleum-derived materials (Baghaei and Skrifvars 2020; Chen et al. 2020; Halley 2020; Rosenboom et al. 2022; Uusi-Tarkka et al. 2021; Wang et al. 2021). Unlike traditional composites that comprise different material components, both matrix and reinforcing components of ACCs are made entirely of cellulosic material (Baghaei and Skrifvars 2020; Gindl-Altmatter et al. 2012; Huber et al. 2012b; Nishino and Arimoto 2007), negating the need for prior separation when considering end-of-life processing (Baghaei and Skrifvars 2020; Mat Salleh et al. 2017; Uusi-Tarkka et al. 2021). Furthermore, cellulose is a biopolymer found abundantly in nature, and the use of renewable or waste biomass is of particular importance in light

**Supplementary Information** The online version contains supplementary material available at <https://doi.org/10.1007/s10570-023-05535-8>.

A. Victoria · P. J. Hine · M. E. Ries (✉)  
School of Physics and Astronomy, University of Leeds,  
Woodhouse Lane, Leeds LS2 9JT, UK  
e-mail: M.E.Ries@leeds.ac.uk

K. Ward  
School of Chemical and Process Engineering, University  
of Leeds, Woodhouse Lane, Leeds LS2 9JT, UK

of growing concerns regarding climate change and resource scarcity (Uusi-Tarkka et al. 2021). In addition to possessing excellent mechanical properties (Nishino et al. 2004) and thermal stability (Baghaei and Skrifvars 2020), cellulose is renewable and biodegradable (Baghaei and Skrifvars 2020; Chen et al. 2020; Zhao et al. 2008), making it a favorable choice of polymer in the development of sustainable materials. The recycling potential and use of bio-based composites place ACC research at the forefront of technological development and a promising option for materials innovation.

As cellulose does not melt (Adu et al. 2021; Bazbouz et al. 2019; Chen et al. 2020; Misra et al. 2011; Nishino et al. 2004), alternative processing is required in the form of dissolution using an appropriate solvent. There are two common methods used to prepare ACCs based on this process. The original concept was presented by Nishino et al. (2004), who described a two-step impregnation method where cellulosic fibres were placed into a solution of fully dissolved cellulosic material. A one-step process was later developed by Gindl and Keckes (2005) based on partial dissolution, whereby a single source of cellulose selectively dissolves in the solvent, allowing an undissolved inner core to remain as the reinforcement. The reinforcement is then surrounded by a matrix produced from the dissolved portion. Since the publication of these seminal works, there has been a steady flow of research in the field of ACCs, from applications in the development of films (Duchemin et al. 2009; Huber et al. 2012b; Nishino and Arimoto 2007; Nishino et al. 2004), to the use of cellulosic textiles to create thicker structures (Baghaei et al. 2020; Baranov et al. 2021; Haverhals et al. 2011; Huber et al. 2012a, 2012b; Mat Salleh et al. 2017; Victoria et al. 2022).

In our previously published work (Victoria et al. 2022), ACCs were produced using cotton textile in combination with interleaved cellulosic films to produce ACCs with enhanced interlaminar adhesion and an excellent balance of mechanical properties. It was found that at relatively high temperatures and short processing times, ACCs could be produced via dissolution in a combination of ionic liquid 1-ethyl-3-methylimidazolium acetate ([C2MIM][OAc]), and dimethyl sulfoxide (DMSO), possessing optimal consolidation when using a 3:1 solvent to cellulose weight (S/C) ratio. Ionic liquids (ILs) are a good

choice of solvent owing to their thermal stability, low melting points and significantly low vapor pressure (Chen et al. 2020; Hauru et al. 2012; Odalanowska et al. 2021; Pinkert and Kenneth 2008). In addition to being considered a more environmentally-friendly route to cellulose dissolution (Ghandi 2014; Swatloski 2002), ILs can dissolve cellulose without prior derivation (Sescousse et al. 2010; Spörl et al. 2018; Uusi-Tarkka et al. 2021) or pre-treatment (Hawkins et al. 2021), increasing process efficiency. A high temperature of 100 °C promotes rapid dissolution, allowing sufficient matrix to be produced in 10 min. It was found that significant improvements in peel strength, a measure of interlaminar strength, could be achieved by using interleaved films, and Young's modulus could be increased by up to twofold (Victoria et al. 2022).

In the drive to develop commercial feasibility for ACCs, functionality and process optimization are key factors to consider. It is of interest to explore the effects of these factors to further understand their contribution to ACC properties, and potentially identify a new optimum set of conditions that can yield properties beyond those currently obtained. It is well known that process conditions play an important role in the resulting properties of composite materials (Kandar and Akil 2016; Ku et al. 2011; Kumar and Balachandar 2014). From a sustainable manufacturing point of view, finding a balance between product functionality and process feasibility is extremely important to ensure the best quality product can be achieved whilst minimising costs and processing times (Harmsen 2014).

Statistical design of experiments (DoE) is an approach used for process optimisation that allows multiple influential factors to be analysed simultaneously, whilst keeping the total number of experimental runs to a minimum (Lee et al. 2022; Mohammed et al. 2020; Montgomery 2017; Vanaja and Shobha Rani 2008; Weissman and Anderson 2014). A great deal of insight can be gained from a carefully structured set of factor combinations, allowing conclusions to be drawn about their influence on a specific output parameter (Lee et al. 2022). DoE offers a more desirable route to process understanding than traditional trial and error or one-factor-at-a-time (OFAT) methods. Here, all factors are fixed except for the one being varied. Once optimized, this factor is fixed for subsequent experiments where another factor is then

varied, and the process continues until all factors have been optimized (Lee et al. 2022; Owen et al. 2001; Weissman and Anderson 2014). In the absence of a pre-planned set of experiments, the ability to truly optimise a process using this approach is inhibited by researcher bias and initial decisions driving the starting point of factors to fix, and those to vary (Weissman and Anderson 2014).

DoE has been used widely across the pharmaceutical industry to optimise product formulations and improve product quality (Fukuda et al. 2018; Gujral et al. 2018; Vanaja and Shobha Rani 2008; Vanaret et al. 2021). The versatility of DoE, however, allows its applications to extend into a wide range of industries such as food production (Favre and Chaves Neto 2021), steel processing (Gunaraj and Murugan 1999; Noordin et al. 2004), biomass extraction (Liao et al. 2007; Mohammed et al. 2020) and biofuel production (Vicente et al. 1998). In the materials industry, the use of DoE has been discussed as a route to optimise composite performance in various manufacturing processes such as resin transfer moulding (RTM) (Garnier et al. 2010) and heat press forming (Kandar and Akil 2016; Tholibon et al. 2017). Composites with traditional reinforcements such as carbon fibre (Garnier et al. 2010) and glass fibre (Kumar and Balachandar 2014) have been of interest, as well as natural fibre reinforced composites (NFRCs) reinforced with flax (Kandar and Akil 2016), coir (Romli et al. 2012), and kenaf (Azmi et al. 2017; Tholibon et al. 2017). Hot compaction is used widely in composites production (Todor et al. 2021) where temperature, pressure, and time are influential factors in the resulting mechanical properties (Kandar and Akil 2016; Kumar and Balachandar 2014). It has, therefore, been the subject of several experimental design studies with respect to the production of composites comprising wood/rubber (Jun et al. 2008), glass/PP (Kumar and Balachandar 2014), flax/PLA (Kandar and Akil 2016), and kenaf/PP (Tholibon et al. 2017).

Despite the growing interest in applying DoE to the manufacture of composite materials, its application in the field of ACCs is in its infancy, with only two reported studies (Kidwai et al. 2020; Mat Salleh et al. 2017) that we are aware of. This study builds on these important works by assessing the robustness of experimental design methods through validation of identified optimum conditions which, to the best of our knowledge, has not been previously reported.

By exploring DoE in the context of our previously reported ACC preparation method, we gain insights into its usefulness as an efficient route to improved process understanding for all methods of ACC production, and as a tool to identify a region of desirable process conditions that may otherwise not be found using traditional methods. This supports the research community in being aware of the tools available to help advance cellulosic science into product realization.

Initially a full factorial design is used to explore the influence of processing time, temperature, and pressure to identify any potential synergistic effects that exist between them and investigate how they might influence ACC mechanical properties. Full factorial designs are commonly used as a screening stage (Montgomery 2017), and have been applied to the exploration of different materials in the composites industry to explore responses such as mechanical properties (Tholibon et al. 2017), impact behaviour (Filho et al. 2022), and machinability (Azmi et al. 2017). A full factorial design typically includes experimental runs carried out at all the highest-level settings, all the lowest level settings, as well as combinations of both, allowing all possible combinations of factors and levels to be tested (Lee 2019; Montgomery 2017; Owen et al. 2001). This helps to assess the feasibility of the extreme conditions of a process and confirm that the design space within which they lie is acceptable.

In the second phase of this work, application of a central composite design was employed. Central composite designs are a form of response surface methodology (RSM), an approach that allows the estimation of second order (quadratic) effects through the inclusion of additional design points within the experimental domain (Box and Wilson 1951; Lee 2019; Zhou and Xu 2017). These designs are useful if curvature is suspected within a system, that a full factorial design cannot accurately estimate with corner points alone. With the ability to estimate curvature, response surface models have some predictive power, making them ideal for optimisation (Errore et al. 2017; Kidwai et al. 2020; Lee 2019). There are different ways to approach central composite designs depending on the system under investigation. An inscribed central composite design (CCI) was employed in this work that would allow additional design points to be specified within the original experimental domain rather

than beyond it to avoid any loss in ACC quality from unsuitable process conditions.

The aims of this study are therefore twofold. First, to perform an assessment of a DoE methodology to a system where some knowledge has already been gained on suitable ranges for the key design parameters. Secondly, to explore whether DoE can help identify a new set of optimized processing variables not previously found, thus highlighting the potential for DoE to advance the research beyond development and into commercial feasibility.

## Materials and methods

### Materials

Bleached 100% cotton with a plain weave was used as the cellulosic textile in this study. The textile had an areal density of 135 g/m<sup>2</sup> and a thread count of 120 in both directions, and was purchased from Minerva fabrics, UK. Natureflex 23NP cellulose film with a thickness of 23 µm was used as the interleaf cellulosic film layer and supplied by the Futamura Group. Although the films are supplied containing small additives, they do not appear to affect the dissolution process, and therefore, they were not removed prior to use (Victoria et al. 2022). Ionic liquid [C2MIM][OAc] with

a purity of  $\geq 95\%$  was purchased from ProIonic and co-solvent dimethyl sulfoxide (DMSO), with a purity of  $\geq 99.9\%$ , was purchased from Fisher Scientific.

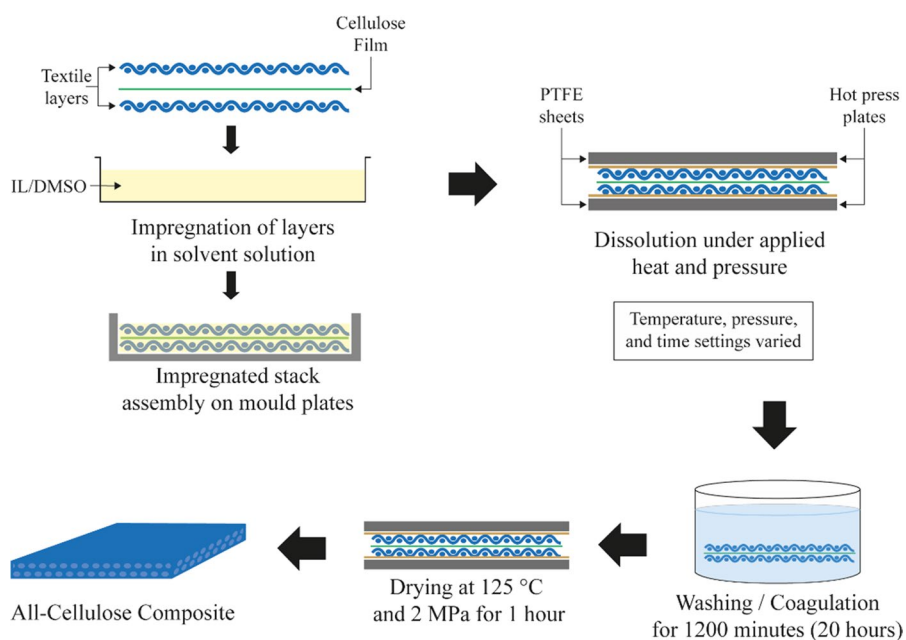
### Composite processing

ACCs were made using two layers of cotton textile and a single layer of Natureflex film placed in-between, and a schematic of the manufacturing stages is provided in Fig. 1.

The cotton textile layers were stacked with respect to the warp yarns at 0°, giving a stacking sequence of (0,0) as shown in Fig. 2. The layers were immersed in a solution of [C2MIM][OAc] and DMSO, and the stack was placed in a laboratory heat press and heated under pressure. The dry mass of cellulose being processed was determined by weighing the textile layers and an S/C weight ratio of 3:1 was used. The solvent solution itself comprised 80% by weight [C2MIM][OAc] and 20% DMSO.

The amount of solvent to use on the stack was determined previously (Victoria et al. 2022), where it was found that a 3:1 S/C weight ratio provided enough solvent to allow sufficient matrix production, and compensate for flashing, where excess cellulose is pushed out under applied pressure. Additionally, adding 20% DMSO significantly lowers the viscosity of [C2MIM][OAc], allowing for ease of application

**Fig. 1** Schematic showing the stages involved in the preparation and manufacture of the ACCs



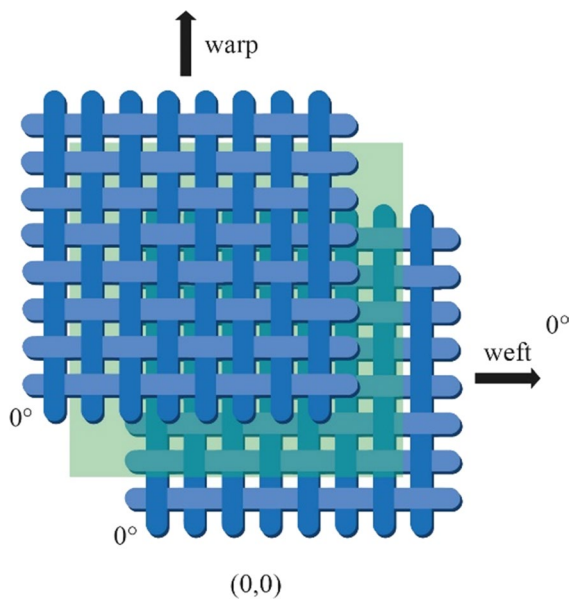


**Fig. 2** Textile stacking arrangement of 0,0 used in the preparation of ACCs, where the warp yarns of both layers are aligned in the same direction

to the textile stack. After dissolution, the samples were left for 1200 min (20 h) in a coagulation bath of distilled water at room temperature, to allow the solvent to be removed. After solvent removal, the stack was placed in the heat press once more to be dried. For this study, processing factors of temperature, pressure and time during compaction were of primary interest and varied as part of the experimental design. The drying stage was fixed at a temperature, pressure, and time of 125 °C, 2 MPa and 60 min respectively, in accordance with previous work (Victoria et al. 2022) and initial development of the process (Hine and Ries 2020).

### Mechanical testing

Mechanical properties of tensile strength, Young's modulus and failure strain were evaluated using an Instron 5584 universal tensile tester according to ASTM D1846. Specimens were cut to a width of 5 mm with a gauge length of 30 mm and tested using a crosshead speed of 10 mm/min. For the optimized samples, T peel strength (ASTM D1876) was tested, using specimens of width and length of 10 mm and 80 mm respectively, and tested at a speed of 80 mm/

min. All specimens were tested in the longitudinal direction, parallel to the direction of the warp yarns.

### Materials characterisation

#### *Density calculations*

Densities of the optimised ACCs were determined using a gravimetric method, by cutting sample specimens and measuring the dimensions using an RS PRO digital caliper to obtain specimen volume. Three specimens were cut for each ACC and weighed to allow for calculation of density. A proposed value of 1.5 g/cm<sup>3</sup> for the density of the cellulosic materials within the ACC was used for comparison, based on previous literature guidance. The absolute density of plant fibres is stated to be between 1.4 and 1.5 g/cm<sup>3</sup> (Mwaikambo and Ansell 2001). The density of cellulose II and bulk amorphous cellulose is estimated as 1.5 g/cm<sup>3</sup> and 1.48–1.5 g/cm<sup>3</sup> (Bawn 1985) respectively.

#### *Optical microscopy*

An Olympus BH2 microscope in reflection mode was used to observe the cross-sections of the prepared ACCs, and measurements of composite thickness were taken from these images using ImageJ. To allow a clear image to be obtained, samples were embedded in epoxy resin and polished. To ensure a consistent and representative view of each sample was obtained, multiple images were collected and used for measurements. An average value for thickness and corresponding standard error was calculated for each ACC sample from six measurements.

### Experimental design

#### *Full factorial design*

To screen the factors of temperature, pressure, and time and explore the potential effects of these factors on the mechanical properties of ACCs, a 2<sup>3</sup> full factorial design was employed. Here, three factors are under investigation, each having 2 levels representing minimum and maximum settings. A preliminary scoping exercise was performed to ascertain the experimental domain within which to conduct experiments, as well as being based on our previously



reported study. Upper and lower limits were determined from operational constraints, whilst also being aware of the importance of maintaining ACC quality. The outcomes of the scoping stage are outlined as follows.

For compaction temperature, a lower limit of 30 °C was chosen to allow accurate maintenance in the laboratory environment, and an upper limit of 150 °C, to remain within a stable temperature range and avoid evaporation of DMSO (O'Neil 2013). For pressure, a lower limit of 1 MPa was chosen to allow efficient compaction of the layers and reduce shape distortion, and an upper limit of 3.6 MPa that could be held consistently throughout the duration of the process. To determine time, several preliminary samples were made at the upper limits for temperature and pressure of 150 °C and 3.6 MPa respectively. It was found that ACC quality could be reasonably maintained without breakage when processed for a maximum of 180 min. Whilst 180 min would be undesirable for an industrial process, it was agreed that using this as an upper time limit would be suitable for this work, to explore a wider design space and obtain the best outcomes from the experimental design. The parameters and coded values of factors are shown in Table 1.

The full factorial design includes 8 factorial runs located at the corner points of the experimental space and a further 5 replicates of the center point of all factor ranges. The center points were replicated 5 times to provide a balanced estimation of error and assessment of repeatability (Lee 2019; Owen et al. 2001). Runs were randomized to reduce the risk of systematic errors. This resulted in 14 experimental runs as shown in Table 2, along with measured responses.

The experimental data obtained for the full factorial design was fitted to a linear model with main effects and interactions, where the predicted mean

**Table 1** Parameters and coded values used in the full factorial design

| Symbol | Factors          | Levels   |         |          |
|--------|------------------|----------|---------|----------|
|        |                  | Low (−1) | Mid (0) | High (1) |
| A      | Temperature (°C) | 30       | 90      | 150      |
| B      | Pressure (MPa)   | 1        | 2.3     | 3.6      |
| C      | Time (mins)      | 1        | 90.5    | 180      |

Actual values used in the experiment are shown

() Coded values are displayed in brackets

**Table 2** Experimental runs used in full factorial design

| Run no | ID       | Factor settings |     |      |
|--------|----------|-----------------|-----|------|
|        |          | A               | B   | C    |
| 1      | 1F (CP)  | 90              | 2.3 | 90.5 |
| 2      | 2F       | 30              | 3.6 | 180  |
| 3      | 3F       | 30              | 3.6 | 1    |
| 4      | 4F       | 30              | 1   | 1    |
| 5      | 5F (CP)  | 90              | 2.3 | 90.5 |
| 6      | 6F       | 30              | 1   | 180  |
| 7      | 7F (CP)  | 90              | 2.3 | 90.5 |
| 8      | 8F       | 150             | 1   | 1    |
| 9      | 9F       | 150             | 1   | 180  |
| 10     | 10F (CP) | 90              | 2.3 | 90.5 |
| 11     | 11F      | 150             | 3.6 | 1    |
| 12     | 12F      | 150             | 3.6 | 180  |
| 13     | 13F (CP) | 90              | 2.3 | 90.5 |
| 14     | 14F (CP) | 90              | 2.3 | 90.5 |

A = Temperature (°C), B = Pressure (MPa), C = Time (mins)

Samples are listed in run order with corresponding sample ID's. Center points are denoted by (CP) next to samples ID

response variable  $\hat{y}_i$ , is written as a linear combination of the factors. The model is shown in Eq. (1) for  $M$  number of independent factors (Lee 2019).

$$\hat{y}_i = \beta_0 + \sum_{j=1}^M \beta_j x_j + \sum_{i < j}^M \sum_{j=1}^M \beta_{ij} x_i x_j \quad (1)$$

where  $x_i$ , and  $x_i x_j$  denote the linear and interaction terms of the independent factor variables, and the coefficients determined when fitting the model for the intercept, linear and interaction terms are represented by  $\beta_0$ ,  $\beta_i$ , and  $\beta_{ij}$ , respectively.

### Response surface design

For optimisation, a subsequent response surface design was established based on the same experimental domain as outlined in Table 3.

Central composite designs (CCD), are a popular form of response surface methodology (RSM) proposed by Box and Wilson (1951). These designs involve the addition of star points, located a certain distance (denoted by  $\alpha$ ) from the centre to allow estimation of curvature and quadratic effects (Lee 2019). The original form of the central composite design is the central composite circumscribed

**Table 3** Parameters and coded values used in the response surface design

|  | Symbol | Factors                            | Levels            |          |         |       |                   |
|--|--------|------------------------------------|-------------------|----------|---------|-------|-------------------|
|  |        |                                    | Low ( $-\alpha$ ) | ( $-1$ ) | Mid (0) | (1)   | High ( $\alpha$ ) |
| Actual values used in the experiment are shown | A      | Temperature ( $^{\circ}\text{C}$ ) | 30                | 53       | 90      | 127   | 150               |
|  | B      | Pressure (MPa)                     | 1                 | 1.5      | 2.3     | 3.1   | 3.6               |
| ( ) Coded values displayed in brackets         | C      | Time (mins)                        | 1                 | 35.7     | 90.5    | 145.3 | 180               |

(CCC), a five-level design where the star points lie at the extreme values of the factors under investigation (Cevheroğlu Çıra et al. 2016), typically extending beyond the original limits set by the full factorial. Whilst useful for exploring a wider experimental space, it is not always appropriate or possible to extend the original factor limits. For example, if the new extreme settings were impractical for a particular process, or might cause quality degradation (Cevheroğlu Çıra et al. 2016; Dozie and Nwanya 2020). An inscribed central composite design (CCI) was chosen for this work, where each factor has five levels, and the upper limits of the original full factorial represent the limits of the CCI design. This creates a design where the additional star points fall inside the experimental domain. The response surface model is shown in Eq. (2) where  $x_i^2$  denotes the additional quadratic term of the independent factor variables, and  $\beta_{ii}$  represents the coefficients determined when fitting the model for quadratic terms.

$$\hat{y}_i = \beta_0 + \sum_{j=1}^M \beta_j x_{ij} + \sum_{i < j}^M \sum_{j=1}^M \beta_{ij} x_i x_j + \sum_{i=1}^M \beta_{ii} x_i^2 \quad (2)$$

The design consisted of 14 additional runs shown in Table 4, along with six center point replicates giving a total of 20 runs. The six center points prepared previously during the full factorial design were used in this design.

### Statistical analysis

The software package Minitab was used to generate the initial full factorial and subsequent response surface designs, as well as analysing the experimental data through regression analysis and analysis of variance (ANOVA). A model was generated from backward elimination of insignificant terms, determined using the  $p$  values ( $p \geq 0.05$  considered insignificant). Coefficient of determination,  $R^2$ , was calculated to

**Table 4** Additional experimental runs used in response surface design

| Run No | Sample ID | Factor settings |     |       |
|--------|-----------|-----------------|-----|-------|
|        |           | A               | B   | C     |
| 1      | 1C        | 30              | 2.3 | 90.5  |
| 2      | 2C        | 90              | 2.3 | 180.0 |
| 3      | 3C        | 90              | 1.0 | 90.5  |
| 4      | 4C        | 90              | 2.3 | 1.0   |
| 5      | 5C        | 150             | 2.3 | 90.5  |
| 6      | 6C        | 90              | 3.6 | 90.5  |
| 7      | 7C        | 53              | 1.5 | 35.7  |
| 8      | 8C        | 127             | 3.1 | 35.7  |
| 9      | 9C        | 53              | 3.1 | 145.3 |
| 10     | 10C       | 127             | 1.5 | 145.3 |
| 11     | 11C       | 127             | 3.1 | 145.3 |
| 12     | 12C       | 127             | 1.5 | 35.7  |
| 13     | 13C       | 53              | 1.5 | 145.3 |
| 14     | 14C       | 53              | 3.1 | 35.7  |

A = Temperature ( $^{\circ}\text{C}$ ), B = Pressure (MPa), C = Time (mins)

Samples are listed in run order with corresponding sample IDs

validate how well the experimental data are represented by the independent terms of the model (de Oliveira et al. 2018; Filho et al. 2022; Mohammed et al. 2023). The adjusted coefficient of determination,  $R^2_{(\text{adj})}$ , used to validate the strength of model with respect to the number of model terms (Montgomery 2017). Additionally, the predicted coefficient of determination,  $R^2_{(\text{pred})}$  was used to gauge the predictive power of the resulting model (Mohammed et al. 2020).

### Response optimization and validation

Derringers desirability function (Derringer and Suich 1980) was used to identify the optimum process conditions to yield the most desirable response. ACC samples were made using these conditions and tested

to determine how well the obtained model was at predicting the properties of additional ACCs.

## Results and discussion

Statistical analysis of the full factorial design

### Tensile Strength

**Table 5** Measured responses from the experimental runs of the full factorial design. Additional responses for each sample can be found in Table SI 1 of the supplementary information

| Run No | ID       | Factor settings |     |      | Responses              |                       |                |                                      |                  |
|--------|----------|-----------------|-----|------|------------------------|-----------------------|----------------|--------------------------------------|------------------|
|        |          | A               | B   | C    | Tensile Strength (MPa) | Young's Modulus (GPa) | Thickness (mm) | Density, $\rho$ (g/cm <sup>3</sup> ) | Void content (%) |
| 1      | 1F (CP)  | 90              | 2.3 | 90.5 | 75.4±3.5               | 3.3±0.2               | 0.23±0.02      | 1.39±0.01                            | 7.3±0.4          |
| 2      | 2F       | 30              | 3.6 | 180  | 67.3±1.5               | 2.5±0.2               | 0.26±0.02      | 1.20±0.01                            | 20.2±0.3         |
| 3      | 3F       | 30              | 3.6 | 1    | 62.3±1.7               | 1.9±0.2               | 0.33±0.02      | 0.96±0.01                            | 35.9±0.4         |
| 4      | 4F       | 30              | 1   | 1    | 47.3±2.3               | 1.4±0.1               | 0.34±0.02      | 0.96±0.01                            | 35.8±0.3         |
| 5      | 5F (CP)  | 90              | 2.3 | 90.5 | 75.4±2.1               | 3.5±0.8               | 0.22±0.01      | 1.39±0.01                            | 7.6±0.9          |
| 6      | 6F       | 30              | 1   | 180  | 58.8±1.5               | 2.4±0.0               | 0.28±0.02      | 1.09±0.01                            | 27.7±0.9         |
| 7      | 7F (CP)  | 90              | 2.3 | 90.5 | 73.8±4.6               | 3.3±0.2               | 0.23±0.02      | 1.33±0.04                            | 11.6±2.5         |
| 8      | 8F       | 150             | 1   | 1    | 23.3±1.1               | 3.1±0.2               | 0.28±0.01      | 1.13±0.04                            | 24.8±2.9         |
| 9      | 9F       | 150             | 1   | 180  | 64.2±3.0               | 3.9±0.1               | 0.19±0.02      | 1.48±0.01                            | 1.6±0.9          |
| 10     | 10F (CP) | 90              | 2.3 | 90.5 | 83.1±1.7               | 3.6±0.1               | 0.24±0.01      | 1.32±0.03                            | 12.1±1.7         |
| 11     | 11F      | 150             | 3.6 | 1    | 46.5±1.9               | 3.8±0.1               | 0.25±0.01      | 1.29±0.02                            | 13.9±1.2         |
| 12     | 12F      | 150             | 3.6 | 180  | 74.2±1.0               | 3.8±0.1               | 0.21±0.01      | 1.30±0.03                            | 13.1±1.7         |
| 13     | 13F (CP) | 90              | 2.3 | 90.5 | 67.4±4.8               | 3.2±0.2               | 0.22±0.01      | 1.35±0.02                            | 10.4±1.2         |
| 14     | 14F (CP) | 90              | 2.3 | 90.5 | 81.2±1.4               | 3.3±0.4               | 0.22±0.01      | 1.33±0.03                            | 11.4±1.8         |

A = Temperature (°C), B = Pressure (MPa), C = Time (mins)

**Table 6** Analysis of Variance (ANOVA) from the full factorial model for tensile strength

| Source                | Degrees of freedom | Sum of squares | Mean square | F-Value | P-Value |
|-----------------------|--------------------|----------------|-------------|---------|---------|
| Model                 | 7                  | 1807.23        | 258.18      | 0.87    | 0.581   |
| A: Temp (°C)          | 1                  | 94.3           | 94.3        | 0.32    | 0.596   |
| B: Pressure (MPa)     | 1                  | 404.02         | 404.02      | 1.37    | 0.295   |
| C: Time (mins)        | 1                  | 904.91         | 904.91      | 3.06    | 0.14    |
| AB                    | 1                  | 11.73          | 11.73       | 0.04    | 0.85    |
| AC                    | 1                  | 338.47         | 338.47      | 1.15    | 0.333   |
| BC                    | 1                  | 48.42          | 48.42       | 0.16    | 0.702   |
| ABC                   | 1                  | 5.38           | 5.38        | 0.02    | 0.898   |
| Residual              | 5                  | 1477.07        | 295.41      |         |         |
| Curvature             | 1                  | 1320.37        | 1320.37     | 33.7    | 0.004   |
| Pure error            | 4                  | 156.7          | 39.17       |         |         |
| Total                 | 12                 | 3284.3         |             |         |         |
| R <sup>2</sup>        |                    | 0.5503         |             |         |         |
| R <sup>2</sup> (adj)  |                    | 0              |             |         |         |
| R <sup>2</sup> (pred) |                    | 0              |             |         |         |



As shown in Table 5 it was not possible to derive a model for tensile strength through the full factorial design. All model terms were insignificant ( $p > 0.05$ ), and the model indicator was also insignificant ( $p = 0.060$ ) as shown in Table 6. The fit statistics of  $R^2$ ,  $R^2_{(adj)}$  and  $R^2_{(pred)}$  were 0.55, 0 and 0 respectively, further highlighting the inadequacy as a model. Although curvature was suspected ( $p < 0.05$ ), the lack of other valid fit statistics suggests that a higher order model may not yield a better estimation. Data transformations (box-cox, square root and log) (Osborne 2010) were also attempted; however, these did not improve the ability of the data to fit a model.

Whilst unsatisfactory from a statistical point of view, the lack of model for tensile strength provides supporting evidence of some stability during processing, such that this parameter is insensitive to a very wide range of processing variables. In our previous work (Victoria et al. 2022), it was demonstrated that adding an interleaf cellulosic film in between textile layers provides an extra source of cellulose that fully dissolves to form the matrix component. This matrix component is sufficient to effectively bond the textile layers together and impregnate the fibre assembly, forming a well consolidated ACC with efficient load

transfer to the partially dissolved fibres. With a dissolution-driven process under applied pressure, there is opportunity for dissolved cellulose and solvent to be lost through flashing, and by using a 3:1 S/C ratio it is possible to ensure that despite this loss, enough solvent is present to fully dissolve the film and only partially dissolve the fibres. Whilst the amount of matrix fraction and ACC consolidation may vary depending on process conditions, the fibre fraction in the ACC is unlikely to change significantly, even at high temperatures where the rate of dissolution is increased (Liang et al. 2020). This explains the lack of significant variation in tensile strength, given this parameter is governed primarily by the fibre fraction of the composite (Matthews and Rawlings 1999; Nagavally 2017).

A plot of Young's modulus and tensile strength for all prepared ACC samples is presented in Fig. 3 where samples are plotted in order of ascending Young's modulus. As Young's modulus increases, tensile strength appears to display an upward trending curve with the exception of samples 8F and 11F, both prepared at temperature and time settings of 150 °C, and 1 min respectively. Both samples have tensile strength values lower than the suggested curve would suggest, particularly sample 8F that

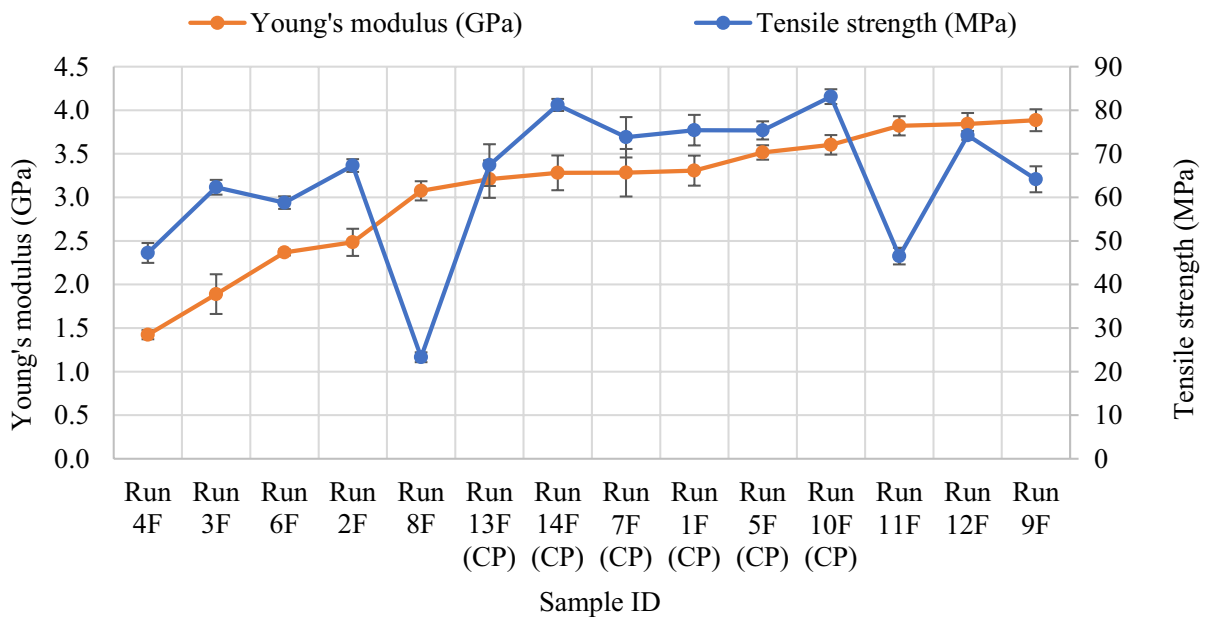


**Fig. 3** Young's modulus and tensile strength of ACC samples prepared for the full factorial design, in order of ascending Young's modulus. Sample 4F was prepared at the lowest tem-

perature and shortest time, and sample 9F was prepared at the highest temperature and the longest time. (CP) denotes runs prepared at the center points

has a notably lower value of  $23 \pm 1$  MPa. Whilst it is possible that this sample is simply an outlier, it could be suggested that the combination of maximum temperature ( $150\text{ }^{\circ}\text{C}$ ) and such a short processing time results in rapid dissolution of the cellulose and a buildup of matrix fraction that cannot be expelled as flash. Although this results in more matrix fraction, the reduced pressure prevents this from being utilized effectively and fully penetrating through the fibre assembly. The insufficient consolidation would cause a decrease in tensile strength. However, the significance of this is not highlighted in the ANOVA, suggesting that within the scope of the full factorial design, there is insufficient data to form a robust conclusion.

It is also worth noting sample 4F, prepared at the lowest temperature and shortest time, and sample 9F, prepared at the highest temperature and the longest time, exhibit the lowest and highest Young's modulus values, respectively. In addition to minimum and maximum factor settings, samples were also prepared at the mid points of all factors and replicated for error estimation, referred to as center points. It is interesting to note from Fig. 3 that the curve in tensile strength appears to maximize for the sample produced at these points. The values for Young's modulus that exceed the center points are obtained for samples 11F, 12F, and 9F, all prepared at the maximum temperature setting of  $150\text{ }^{\circ}\text{C}$ , and two of these samples were prepared at the maximum time setting of 180 min. Whilst the Young's modulus values obtained at the center points are not as high as these samples, they are close. In addition, the tensile strength of the center

points is more noticeably higher, providing the best balance of properties from all factor combinations. This suggests that the largest overall improvement could be obtained towards the middle of the exploratory space, negating the need for higher temperatures and long dissolution times.

The peak values for tensile strength obtained at the center points is also worth noting in the context of the ANOVA analysis. The average tensile strength across the five center points is  $76 \pm 2$  MPa; the maximum value obtained from all sample runs, and the coefficient of variance (COV) across the center points for tensile strength was 7%. Whilst being under 10% supports process reproducibility, a value above 5% is nonetheless a reflection on the inherent variability of natural fibres such as cotton (Awais et al. 2021; Tholibon et al. 2017). One of the key limitations of a 2-level full factorial design is the inability to estimate quadratic effects (Azmi et al. 2017; Jones and Nachtsheim 2011; Lee et al. 2022). If there is very little variation between extreme corner points, a full factorial design will inevitably not pick up any changes in between. Although the addition of center points can help detect local curvature (Lee 2019), the variation in the majority of values obtained for tensile strength reflect overall, the marginal variations in this parameter from lower to upper limits.

#### *Young's modulus*

A first order linear model was fitted for Young's modulus with time and temperature as main effects with

**Table 7** Analysis of Variance (ANOVA) from the Full Factorial model for Young's modulus

| Source                         | Degrees of freedom | Sum of squares | Mean square | F-value | <i>p</i> -value |
|--------------------------------|--------------------|----------------|-------------|---------|-----------------|
| Model                          | 2                  | 5.9172         | 2.95862     | 21.72   | 0.00015         |
| A: Temp ( $^{\circ}\text{C}$ ) | 1                  | 5.2155         | 5.21548     | 38.3    | 0.00007         |
| C: Time (mins)                 | 1                  | 0.7018         | 0.70176     | 5.15    | 0.04431         |
| Residual                       | 11                 | 1.4981         | 0.13619     |         |                 |
| Curvature                      | 1                  | 0.9193         | 0.91935     | 15.88   | 0.00258         |
| Lack-of-Fit                    | 5                  | 0.4579         | 0.09159     | 3.79    | 0.08498         |
| Pure Error                     | 5                  | 0.1208         | 0.02416     |         |                 |
| Total                          | 13                 | 7.4153         |             |         |                 |
| $R^2$                          |                    | 0.798          |             |         |                 |
| $R^2$ (adj)                    |                    | 0.7612         |             |         |                 |
| $R^2$ (pred)                   |                    | 0.6494         |             |         |                 |

no interaction terms. The results of the Analysis of Variance (ANOVA) are shown in Table 7.

For each factor and factor combination in the model, the associated  $p$ -value indicates a significant effect within a confidence range of 95% if less than 0.05 (Filho et al. 2022). Furthermore, the  $p$ -value for the model indicator is significant ( $p < 0.05$ ), suggesting that the model is a good fit to the experimental data (Filho et al. 2022; Mohammed et al. 2023; Montgomery 2017). Additional statistical indicators such as  $F$ -value can be used to further support the confidence in the derived model (Mohammed et al. 2023, 2020), for example the  $F$ -value of 3.79 and  $p$ -value of 0.08 for the lack of fit indicates that the model is statistically insignificant relative to pure error. Finally,  $R^2$ ,  $R^2_{(adj)}$ , and  $R^2_{(pred)}$  were 0.80, 0.76, and 0.65 respectively, and the difference between  $R^2_{(adj)}$  and  $R^2_{(pred)}$  is less than 0.2, which indicates that the model agrees well with the data (Anderson and Whitcomb 2016; Filho et al. 2022; Jankovic et al. 2021; Mohammed et al. 2023; Oliveira et al. 2018). Based on these indicators, it was agreed that the model for Young's modulus was statistically acceptable, and Young's modulus could be estimated with a linear model as given in Eq. (3), where  $A$  and  $C$  are temperature in  $^{\circ}\text{C}$  and time in minutes, respectively. The model is given in the form of uncoded factors, where the independent variables of temperature, pressure and time are

expressed in their real units, rather than coded units such as  $-1$ ,  $0$ ,  $1$  that typically represent the point type in relation to the factor levels in the experimental design (Montgomery 2017).

$$\text{Young's modulus} = 1.526 + 0.01346 A + 0.00331 C \quad (3)$$

Main effects plots are presented in Fig. 4 showing the overall trend in Young's modulus as a function of temperature and time, based on the model estimation. Here, the positive influence of temperature and time is apparent, as well as the comparatively larger effect that temperature has, compared to time. This correlates with the data plots in Fig. 3 which show that the lowest and highest Young's modulus values are obtained from samples 4F, prepared at the lowest temperature and shortest time, and sample 9F, prepared at the highest temperature and the longest time, respectively.

There was, however, as highlighted in Table 7, significant curvature suspected ( $p < 0.05$ ), suggesting that there may be an unknown, further optimized region located within the experimental domain. This echoes the earlier observation made regarding the balance of properties obtained at the center points.

**Fig. 4** Main effects plots for Young's modulus

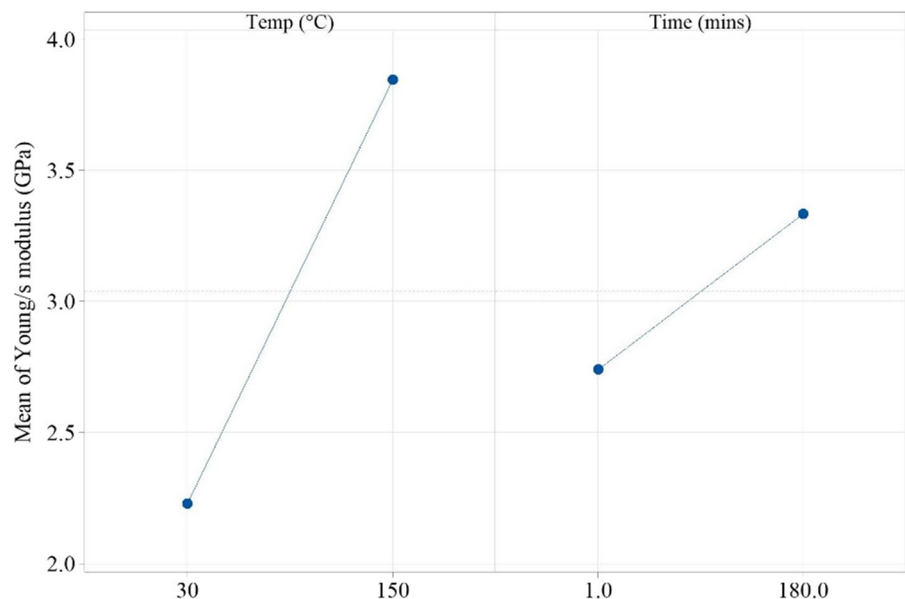
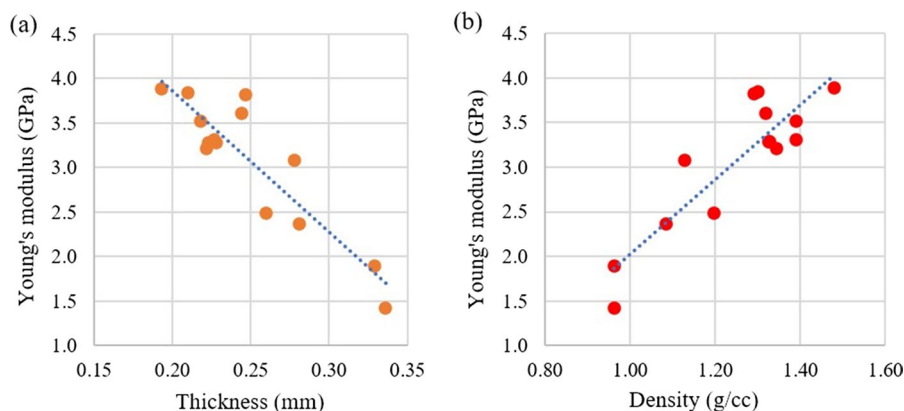


**Fig. 5** Young's modulus of prepared ACCs plotted against. **a** thickness and **b** density



### Analysis of the full factorial data

To explore the reasons behind the estimated trends in Young's modulus, the physical and mechanical properties of the ACC samples were plotted to identify any relationships present. Young's modulus is plotted against ACC thickness and density in Fig. 5, showing strong correlations between these metrics and highlighting the influence of physical properties in driving Young's modulus (Chen et al. 2020; Korhonen et al. 2019). A thinner material is likely due to a reduction of internal void space as air is pushed out under compaction, as well as a reduction in excess matrix fraction as dissolved cellulose is lost. This produces a denser material, which is an important factor to consider in ACC performance (Chen et al. 2020; Korhonen et al. 2019).

The difference in thickness can be seen in the ACC cross-sections obtained from optical microscopy shown in Fig. 6, paying close attention to samples 4F and 9F in Fig. 6a, f, that exhibit the lowest and highest Young's modulus, respectively. These samples were prepared at the minimum and maximum settings for temperature and time, providing some insight into the potential positive influence of the two process factors. The difference in thickness can be seen very clearly between the two samples, where a much thinner, arguably more consolidated ACC cross-section is seen in 9F, prepared at the highest temperature and time settings of 150 °C and 180 min, respectively. The density of this sample is significantly higher as  $1.48 \text{ g/cm}^3$ , as compared to 4F prepared at temperature and time settings of 30 °C and 1 min, respectively.

A comparison of properties for these samples is shown in Fig. 7 along with a visual representation of the two-dimensional space in which these samples lie. The increased density achieved at the highest temperature and time settings additionally indicates a low void content which would contribute to a strong fibre-matrix interface and strong bonding between the layers. This makes for efficient transfer of external loads which is evidenced in the improvement of Young's modulus from  $1.40 \pm 0.05$  to  $3.9 \pm 0.1$  GPa when comparing 4F to 9F. In addition, tensile strength is improved from  $47.3 \pm 2.3$  to  $64.1 \pm 3.0$  MPa between the two samples. The influence of temperature in supporting dissolution is also apparent in Fig. 6a–d where the interleaf film can still be seen between the textile layers. As previously found, complete dissolution of the film is desirable to ensure that the matrix can fully penetrate the fibre assembly and reduce void content. The lower range of density values for all samples prepared at 30 °C supports this, with a range of 0.96–1.20  $\text{g/cm}^3$ .

It is important to be aware of overall product quality when looking to optimise a process. Photographs of each prepared ACC after processing are shown in Fig. 8 where some discolouration of the samples prepared at the highest time settings can be seen, as well as some loss of quality and consistency of the surface.

Whilst it is crucial to look at optimising mechanical properties, maintaining product quality and visual appeal is equally important. Therefore, such desirability attributes must be considered to ensure a good balance of properties can be obtained without compromising quality. The derived linear model for Young's modulus estimates an increase in this property with increased temperature and time, and this reflects the

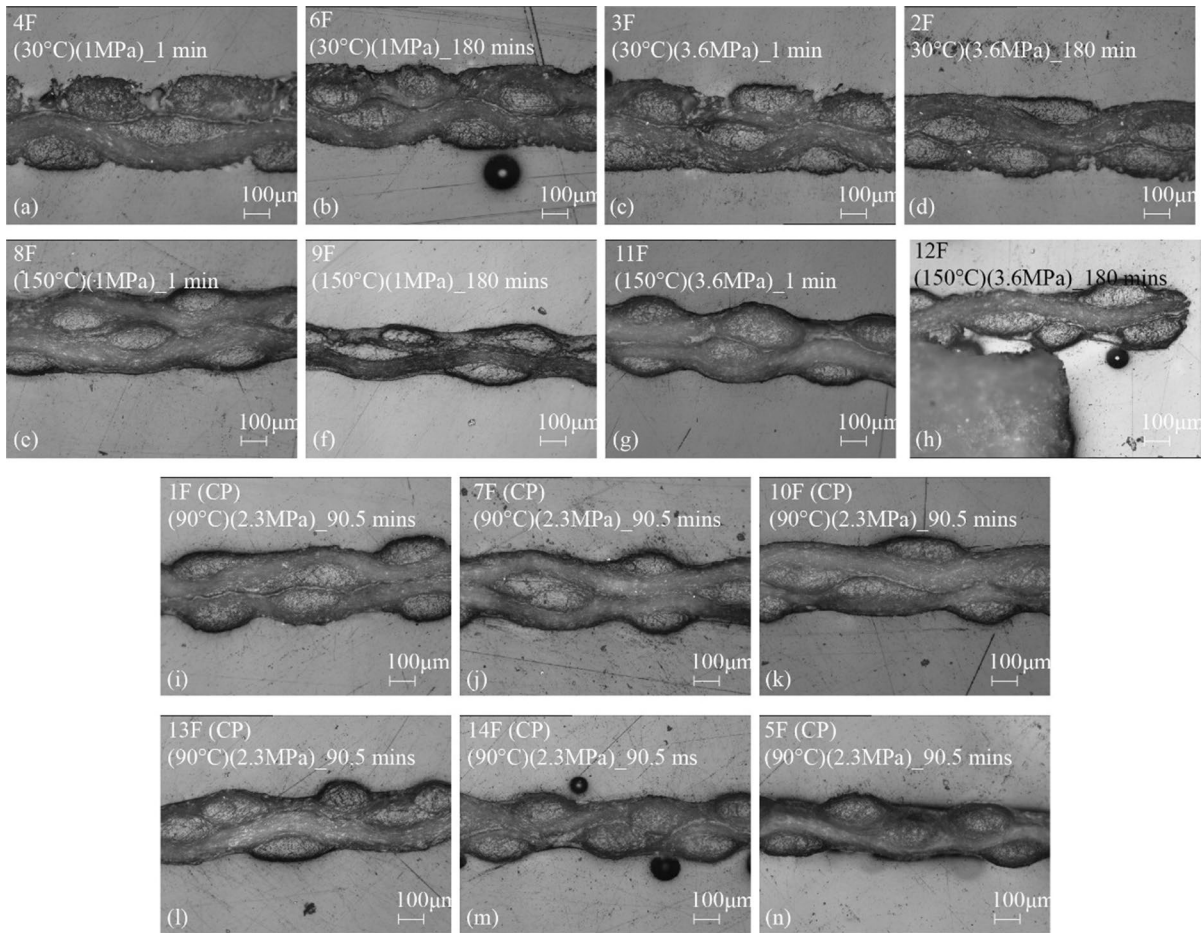


**Fig. 6** Optical microscopy cross-section images of ACCs prepared for the full factorial design including six center points. Samples are labelled in the following way, ID(X)(Y)\_Z representing an ACC prepared at a temperature of X °C, a pressure

of Y MPa, and a time of Z minutes, prefixed with sample ID. CP denotes the samples prepared at the center points. Scale bar represents 100  $\mu\text{m}$

high modulus achieved for sample 9F, irrespective of sample quality.

For a commercial process, dissolution times of 180 min would typically not be favourable, as it is always in the best interest for materials to be produced in the most time-efficient way (Hull and Clyne 1996; Johnson 2003). In addition, the importance of sustainable processing must not be overlooked, and so it would be useful to explore energy requirements associated with processing conditions. From the temperature and time settings for each experimental run, a value can be calculated to represent the heat energy used in production, give in Eq. 4 as follows:

$$\begin{aligned} &\text{Heat energy used in production (C}^\circ \cdot \text{hr)} \\ &= (\text{Temperature (C}^\circ\text{)} - \text{Room temperature (C}^\circ\text{)}) \quad (4) \\ &\quad \times \text{Time (hr)} \end{aligned}$$

Where room temperature in the lab is taken as 20 °C. This then provides a metric to compare the energy used making each sample. The mechanical absorbed energy (toughness) during tensile testing can also be found by calculating the area under the stress–strain plots, to indicate how much energy the material is absorbing as it undergoes tensile loads.



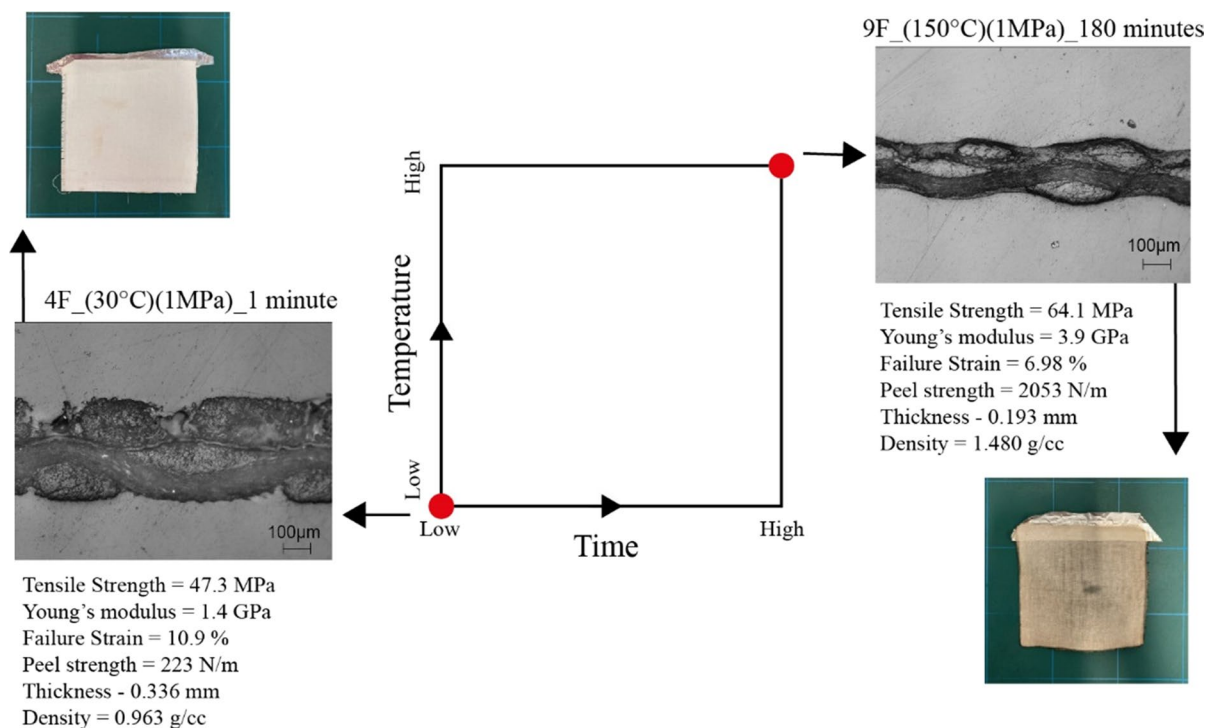


**Fig. 7** Images and comparison of properties of samples prepared at the lowest and highest temperature and time settings in the full factorial design

Figure 9 shows both the heat energy used in production, and mechanical absorbed energy for each sample from the full factorial design, plotted in the same order as shown in Fig. 3, in order of ascending Young's modulus.

From Figs. 3 and 9, this it is seen that although sample 9F possesses the highest modulus, the energy required to produce this sample at maximum temperature and time is significantly higher than that required to produce the center points, for example. Additionally, the energy absorbed for the center points is in the higher range of all samples. These observations further support the suggestion that the optimized region may be located closer to the center of the experimental domain, in terms of reducing energy requirements as well as achieving a good balance of properties. The next phase of this study involves expanding the work to a response surface design to explore the possible curvature and optimum region, and estimate potential higher order quadratic effects (Jankovic et al. 2021).

Statistical analysis of the CCI design

#### *Tensile strength*

Table 8 shows the experimental conditions assigned to the CCI design, along with measured responses. For tensile strength, no terms were significant ( $p > 0.05$ ) and so it was not possible to obtain a response surface model for this property. With five levels for each factor rather than three, the majority of factor combinations for this response surface design combine the settings located at the interior points of the experimental domain.

Where the full factorial design comprised combinations of upper and lower limit settings in one run (corner points), the CCI design omits these. Of the 14 extra experimental runs involved, seven of these comprise just one factor set at its upper or lower limit, and the remaining runs are combinations of the inner levels. It is useful to refer to Fig. 10 where cross-sectional images of the ACCs samples prepared for the CCI design are presented, showing a smaller range of variability in thickness and



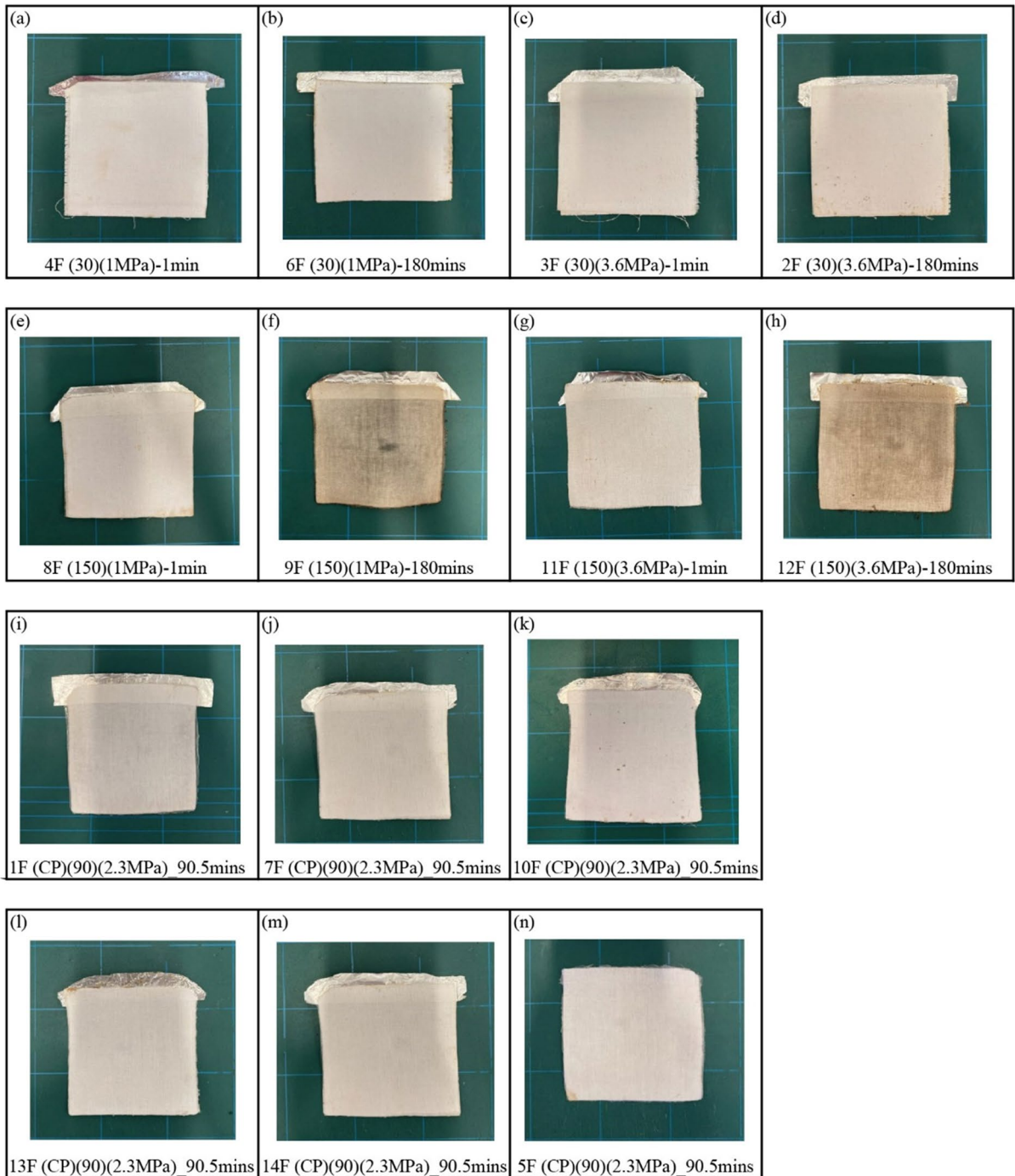


**Fig. 8** Images of ACC samples produced for the full factorial design including six centre points. Samples are labelled in the following way, ID(X)(Y)\_Z representing an ACC prepared at

a temperature of X °C, a pressure of Y MPa, and a time of Z minutes, prefixed with sample ID. (CP) denotes the samples prepared at the centre points

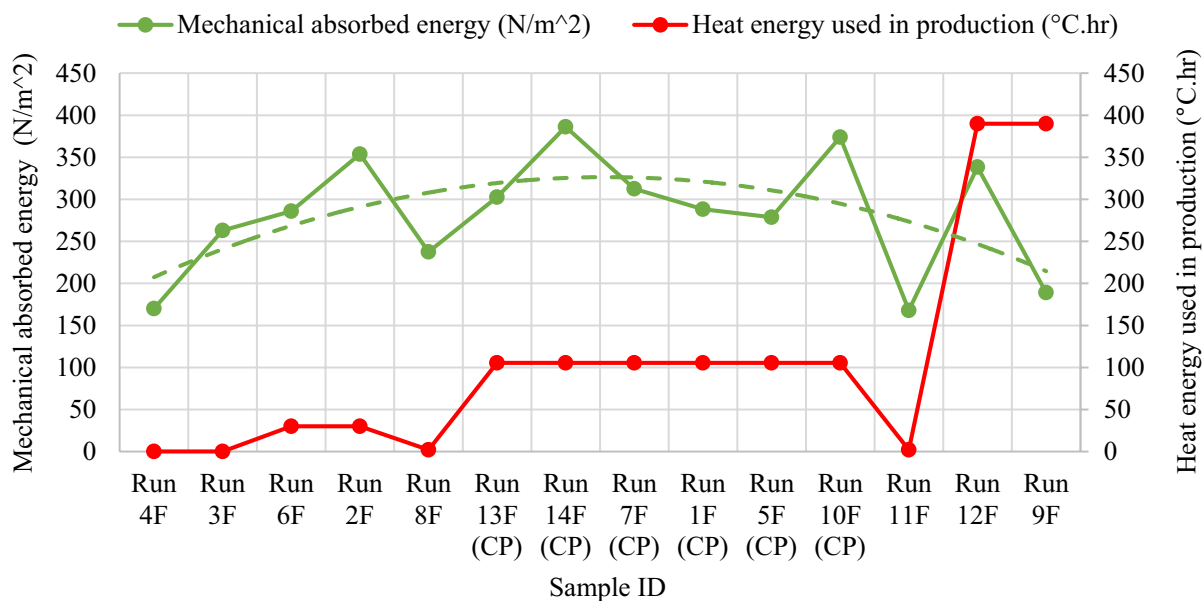


**Fig. 9** Mechanical absorbed energy and heat energy used in production plotted for each ACC sample in order of ascending Young's modulus

**Table 8** Experimental runs used in the response surface design, with responses

| Run No        | Sample ID | Factor settings |     |       | Responses             |                        |
|---------------|-----------|-----------------|-----|-------|-----------------------|------------------------|
|               |           | A               | B   | C     | Young's Modulus (GPa) | Tensile Strength (MPa) |
| 1             | 1C        | 30              | 2.3 | 90.5  | 2.3±0.1               | 56.1±2.4               |
| 2             | 2C        | 90              | 2.3 | 180.0 | 2.9±0.1               | 79.6±1.1               |
| 3             | 3C        | 90              | 1.0 | 90.5  | 3.1±0.0               | 63.2±1.2               |
| 4             | 4C        | 90              | 2.3 | 1.0   | 2.3±0.1               | 68.0±2.0               |
| 5             | 5C        | 150             | 2.3 | 90.5  | 3.0±0.0               | 78.5±2.2               |
| 6             | 6C        | 90              | 3.6 | 90.5  | 3.0±0.1               | 69.8±1.8               |
| 7             | 7C        | 53              | 1.5 | 35.7  | 2.9±0.1               | 73.1±1.7               |
| 8             | 8C        | 127             | 3.1 | 35.7  | 2.9±0.2               | 70.1±1.7               |
| 9             | 9C        | 53              | 3.1 | 145.3 | 2.7±0.1               | 71.3±1.3               |
| 10            | 10C       | 127             | 1.5 | 145.3 | 3.2±0.1               | 73.7±1.9               |
| 11            | 11C       | 127             | 3.1 | 145.3 | 2.8±0.1               | 88.9±5.1               |
| 12            | 12C       | 127             | 1.5 | 35.7  | 2.9±0.2               | 48.9±1.2               |
| 13            | 13C       | 53              | 1.5 | 145.3 | 2.5±0.1               | 62.2±1.5               |
| 14            | 14C       | 53              | 3.1 | 35.7  | 2.7±0.1               | 65.5±0.7               |
| Center Points |           |                 |     |       |                       |                        |
|               | 1F (CP)   | 90              | 2.3 | 90.5  | 3.3±0.2               | 75.4±3.5               |
|               | 7F (CP)   | 90              | 2.3 | 90.5  | 3.3±0.3               | 73.8±4.6               |
|               | 10F (CP)  | 90              | 2.3 | 90.5  | 3.6±0.1               | 83.1±1.7               |
|               | 13F (CP)  | 90              | 2.3 | 90.5  | 3.2±0.2               | 67.4±4.8               |
|               | 14F (CP)  | 90              | 2.3 | 90.5  | 3.3±0.2               | 81.2±1.4               |
|               | 5F (CP)   | 90              | 2.3 | 90.5  | 3.52±0.08             | 75.4±2.1               |

A = Temperature (°C),  
B = Pressure (MPa),  
C = Time (mins)

Samples are listed in run order, and sample IDs are given as XC where X represents run order. Center points from the full factorial design are also included for completeness

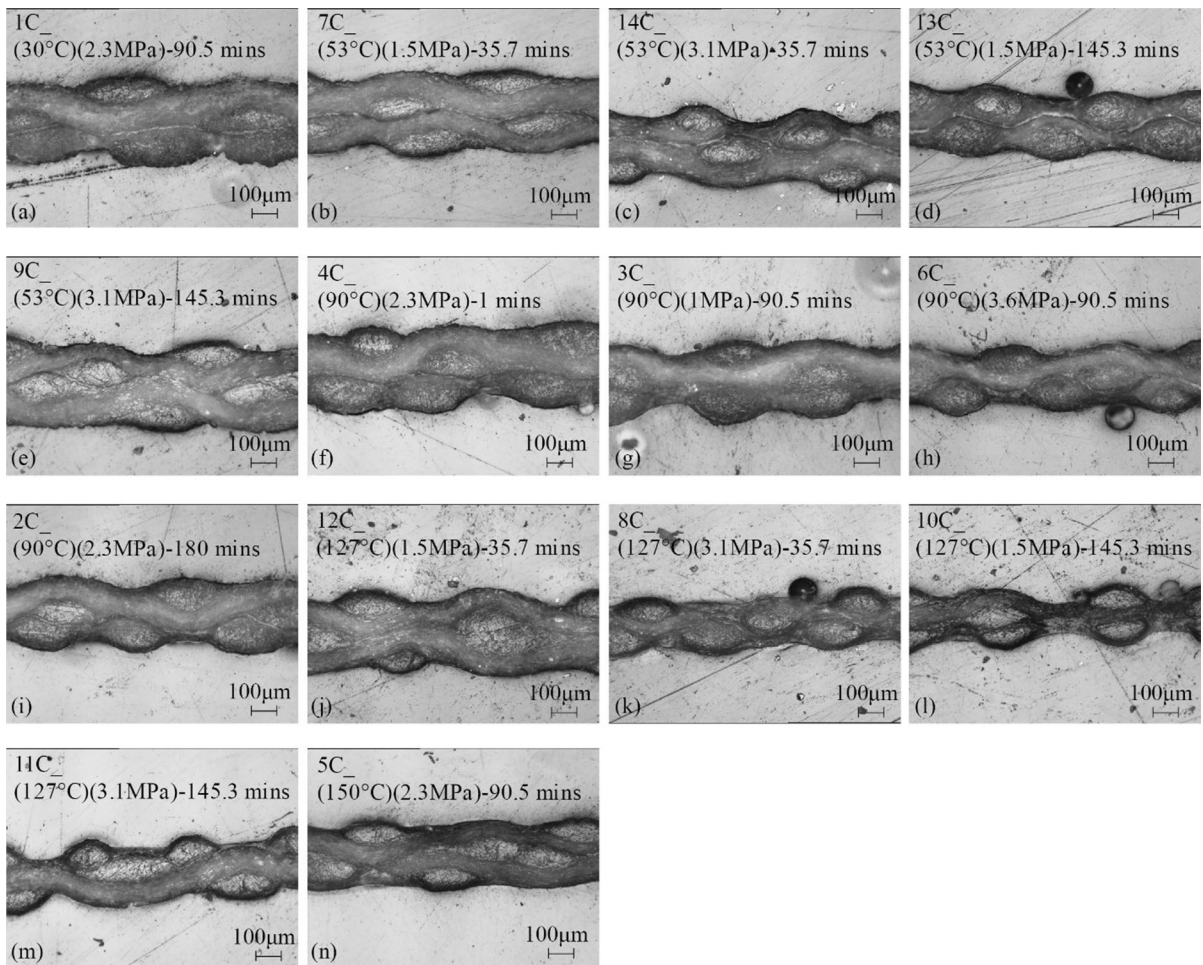


**Fig. 10** Optical microscopy cross-section images of ACCs prepared for the response surface CCI design. As previously for the full factorial design, samples are labelled in the fol-

lowing way, ID(X)Y\_Z representing an ACC prepared at a temperature of X °C, a pressure of Y MPa, and a time of Z minutes, prefixed with sample ID. Scale bar represents 100 μm

consolidation across all samples. This differs from the samples obtained for the full factorial where the consolidation and thickness of the samples were more variable. This is reflected in the lack of modelling power across a relatively small range of values for tensile strength, and further supports the overall stability of this property within the boundaries of the chosen domain.

#### Young's modulus

It was possible to fit a second order quadratic model to the experimental data for Young's modulus as shown in Eq. (5) in the form of uncoded factors, where A, B and C represent temperature in °C, pressure in MPa,

and time in minutes, respectively. The results of the ANOVA analysis are shown in Table 9. For this model,  $R^2$ ,  $R^2_{(adj)}$ , and  $R^2_{(pred)}$  were 0.75, 0.68, and 0.49 respectively, and the difference between  $R^2_{(adj)}$  and  $R^2_{(pred)}$  was again less than 0.2. Additionally, the model is statistically insignificant ( $p > 0.05$ ) relative to lack of fit, as demonstrated by p-value of 0.22 and corresponding F-value of 2.06.

#### Young's modulus

$$= 0.696 + 0.03653 A + 0.01583 C - 0.000180 A^2 - 0.000082 C^2 \quad (5)$$

All coefficients in the model are significant ( $p < 0.05$ ) except for time as a main linear effect.

**Table 9** Analysis of Variance (ANOVA) from the response surface model for Young's modulus

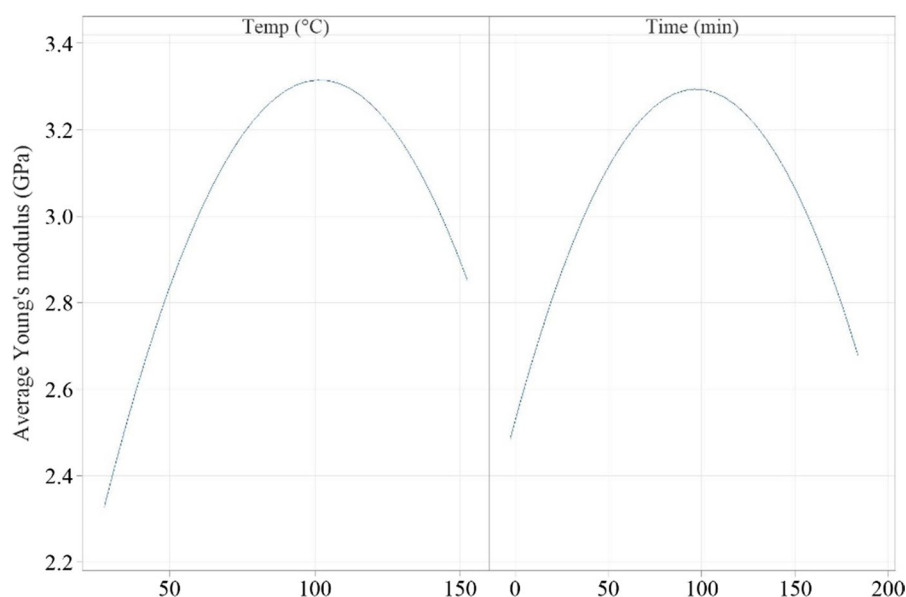
| Source                             | Degrees of freedom | Sum of squares | Mean square | F-value | P-value |
|------------------------------------|--------------------|----------------|-------------|---------|---------|
| Model                              | 4                  | 1.8398         | 0.45995     | 11.17   | 0       |
| A: Temp (°C)                       | 1                  | 0.31424        | 0.31424     | 7.63    | 0.015   |
| C: Time (mins)                     | 1                  | 0.04292        | 0.04292     | 1.04    | 0.323   |
| A <sup>2</sup> : Temp <sup>2</sup> | 1                  | 0.78151        | 0.78151     | 18.98   | 0.001   |
| C <sup>2</sup> : Time <sup>2</sup> | 1                  | 0.79998        | 0.79998     | 19.43   | 0.001   |
| Residual                           | 15                 | 0.61749        | 0.04117     |         |         |
| Lack-of-fit                        | 10                 | 0.49668        | 0.04967     | 2.06    | 0.221   |
| Pure error                         | 5                  | 0.12081        | 0.02416     |         |         |
| Total                              | 19                 | 2.45729        |             |         |         |
| R <sup>2</sup>                     |                    | 0.7487         |             |         |         |
| R <sup>2</sup> (adj)               |                    | 0.6817         |             |         |         |
| R <sup>2</sup> (pred)              |                    | 0.4864         |             |         |         |

However, given the significance of the quadratic effect, this term must be present in the model to maintain hierarchy (Errore et al. 2017; Owen et al. 2001). The significance of temperature and time as main effects found from the full factorial is again indicated in the response surface model and refined to suggest that the significance arises from the quadratic effects more than the linear terms. As found in the initial full factorial design, pressure is deemed insignificant ( $p > 0.05$ ), which is interesting given that the addition of pressure under compaction can reduce void content and improve consolidation

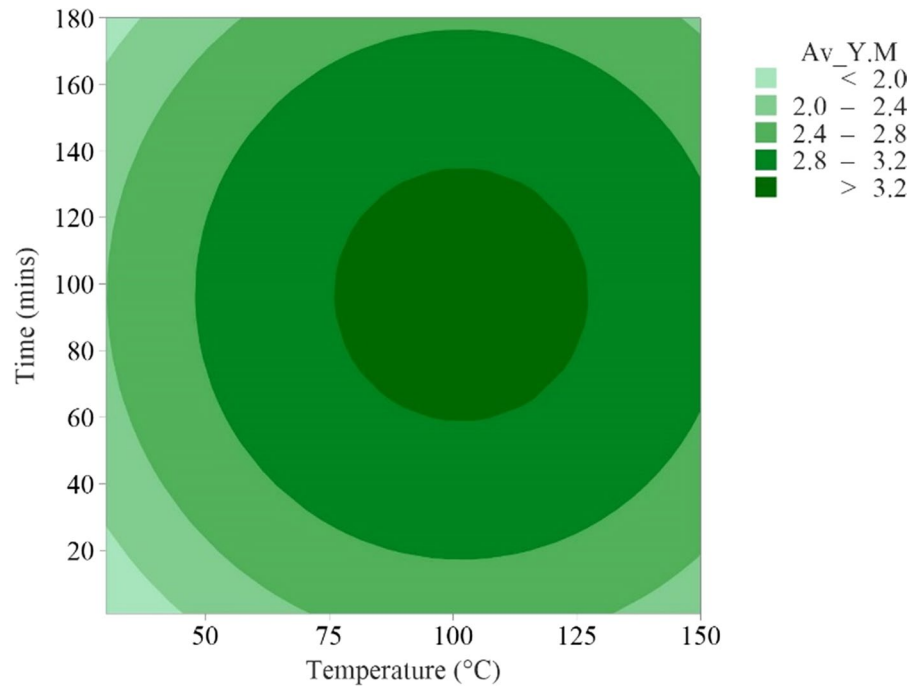
(Huber et al. 2012b; Mat Salleh et al. 2017). It is possible that the chosen pressure range used in this study is sufficient to achieve desired consolidation, and that looking at a wider pressure range in future work could confirm this.

#### Influence of temperature and time on Young's modulus

The main effects plots in Fig. 11 display the quadratic effects of both temperature and time on Young's modulus based on the derived model, and the curvature

**Fig. 11** Main effects plots for Young's modulus as a factor of processing factors temperature and time

**Fig. 12** 2D contour plot of Young's modulus as a function of temperature and time, generated from the statistical model



that was suspected in the full factorial design. An increase in modulus is achieved with increased temperature and time up to a point, after which the property begins to drop. This is also represented through the two-dimensional contour plot in Fig. 12, where the region of optimized modulus lies around the mid-points of temperature and time within the design space.

Achieving a sufficient balance of matrix and fibre reinforcement is key to the functionality of ACCs, and the volume of matrix present after processing relies on how much cellulosic material dissolves, as well as how much is retained under compaction. In previous work, it was hypothesised that a combination of sufficient solvent and high temperature would result in complete dissolution of the film, and partial dissolution of fibre. This would preserve fibre reinforcement and create enough matrix to bond the textile layers together, as well as penetrate the fibre assembly. Sufficient matrix contributes to a strong interfacial bond strength where loads can be transferred efficiently from the matrix to the reinforcing fibers, resulting in good mechanical performance. Extending beyond 100 °C in this work allows for the opportunity to study what happens at lower and indeed, higher temperatures.

The reduced Young's modulus at low temperatures (30–50 °C) suggests that although dissolution occurs, it is not sufficient to fully dissolve the film and allow sufficient matrix to disperse among the fibre assembly. This was evident from the full factorial where the samples produced at the lowest temperature and time settings of 30 °C and 1 min respectively (Fig. 6a, c) showed signs of poor consolidation and incomplete film dissolution. Although there was some improvement at 180 min (Fig. 6b, d), this improvement was minimal. The film can still be seen in Fig. 10a–d in the samples prepared at 30 and 53 °C, although consolidation is arguably improved with the increased time for these samples. Over time there is more opportunity for matrix penetration to happen resulting in a small improvement of properties as suggested in Fig. 12.

Increasing time or temperature to achieve improvements in Young's modulus mirrors previous work into the time–temperature superposition of cellulose dissolution (Hawkins et al. 2021), and is particularly clear at the lower settings of both factors. The optimised region highlights the positive effect of increasing temperature and time within the first 100 min and below 100 °C. Here, the increased temperature results in faster dissolution, which, with an increased time, results in longer compaction



and more consolidation. Beyond this point, it is suggested that increasing one or both factors result in a reverse in the trend and a decrease in modulus which was not picked up in the original full factorial. It can be hypothesised that increased dissolution of the fibre results in a lower fibre volume fraction in the resulting ACC which would contribute to reduced properties. Although arguably more matrix material emerges from increased fibre dissolution, this is pushed out over time, resulting in an uneven composition of fibre and matrix. Looking at Fig. 10m for example, this sample prepared at a high combination of temperature and time is visibly thinner and more uneven than the rest, and there is a distinct lack of sufficient matrix surrounding the fibres.

Limiting fibre dissolution is key to achieving a good balance of mechanical properties, and the cellulosic film offers extra matrix material to allow this to happen. The primary focus is to ensure the processing conditions are sufficient to simply ‘wet’ the fibres so that a strong fibre-matrix interface is created. The optimised region for maximising Young’s modulus is where dissolution is such that a small amount of cellulose is dissolved overall from both precursors. The film dissolves fully due to it being physically thinner, and the fibres within the yarns only partially dissolve the outer fibre layer, leaving the inner core of highly orientated cellulose (Klemm et al. 2005; Soykeabkaew et al. 2009) intact to provide strength.

It is important to remain aware that the trends provided in Figs. 11 and 12 are estimation based on the best fit model obtained through analysis of the measured data. It should be accepted that with all experimental work, there is bound to be variations between the data and the fitted model, and this is particularly relevant when working with natural materials that possess inherent variability. As both the full factorial and the CCI are analysed independently, there may be some variation in each model estimation due to them being based largely on different data sets. For example, the drop in properties at higher temperature and time as estimated from the CCI design, is not as apparent in the full factorial runs, as sample 9F prepared at the maximum temperature and time exhibited a high modulus, rather than a reduced one. In the CCI, the samples prepared at higher temperature and time settings, for example, 10C and 11C, exhibit similar Young’s modulus to the values obtained at the

center points. It could be that in reality the properties are levelling off rather than decreasing. The disparity between the model and the data is a result of the best fit based on most of the available data, bearing in mind that the CCI model estimates from more runs, and thus more data than the full factorial. Overall, the estimations for Young’s modulus are reasonably matched in terms of significant factors, allowing the response surface model obtained from the CCI to bring some insight into how the ACCs can be optimized. The ability to accurately predict properties based on optimised conditions, will be explored in the next section.

### Desirability of model results

The optimum combination of process conditions to maximize Young’s modulus was obtained using Derringer’s desirability function based on the obtained CCI response surface model with a standard deviation of 0.2. Optimum temperature, and time settings of 101 °C and 96.8 min respectively were identified, to produce an ACC with an average Young’s modulus of 3.3 GPa. This is unsurprising when looking at the measured Young’s modulus values across the CCI runs, as the samples exhibiting values at the upper end of the range are indeed the center points, prepared at temperature and time settings close to the desirability prediction. This supports the earlier hypothesis that the more favourable combination of properties may well lie within the mid-range of the processing factors.

As pressure was not deemed significant in the final model, the midpoint of the pressure range was chosen for sample preparation. Five replicates were made and for each replicate, five specimens were tested. The mean, and coefficient of variance across all replicates was then calculated.

### Model validation

Table 10 shows the measured properties of all in-lab test samples, along with coefficient of variance (COV) and standard deviation across replicates. Images of the test samples are shown in Fig. 13. A Young’s modulus of  $3.4 \pm 0.1$  was obtained from five experimental samples, with a COV of 6.2% and standard deviation of 0.2. With a COV of 0.85% between model and experimental values, there is a good



**Table 10** Properties of experimental samples prepared at the identified conditions for optimising Young's modulus, with model prediction for Young's modulus

| Processing conditions       |                |             | n  | Young's modulus (GPa) | S.D  |
|-----------------------------|----------------|-------------|----|-----------------------|------|
| Tem-perature (°C)           | Pressure (MPa) | Time (mins) |    | Average               |      |
| <i>Experimental samples</i> |                |             |    |                       |      |
| 101                         | 2.3            | 96.8        | 5  | 3.4                   | 0.2  |
| 101                         | 1              | 96.8        | 2  | 3.4                   | 0.1  |
| 101                         | 3.6            | 96.8        | 2  | 3.37                  | 0.03 |
| <i>Model prediction</i>     |                |             |    |                       |      |
| 101                         | –              | 96.8        | 20 | 3.3                   | 0.2  |

agreement with the model prediction, demonstrating that the model is capable of successfully predicting the properties of the ACCs and optimizing Young's modulus. Moreover, an independent two-sample t-test ( $p=0.05$ ) was conducted on the model prediction and experimental samples, concluding that the difference between them was not significant (McKillup 2011; Mohammed et al. 2023).

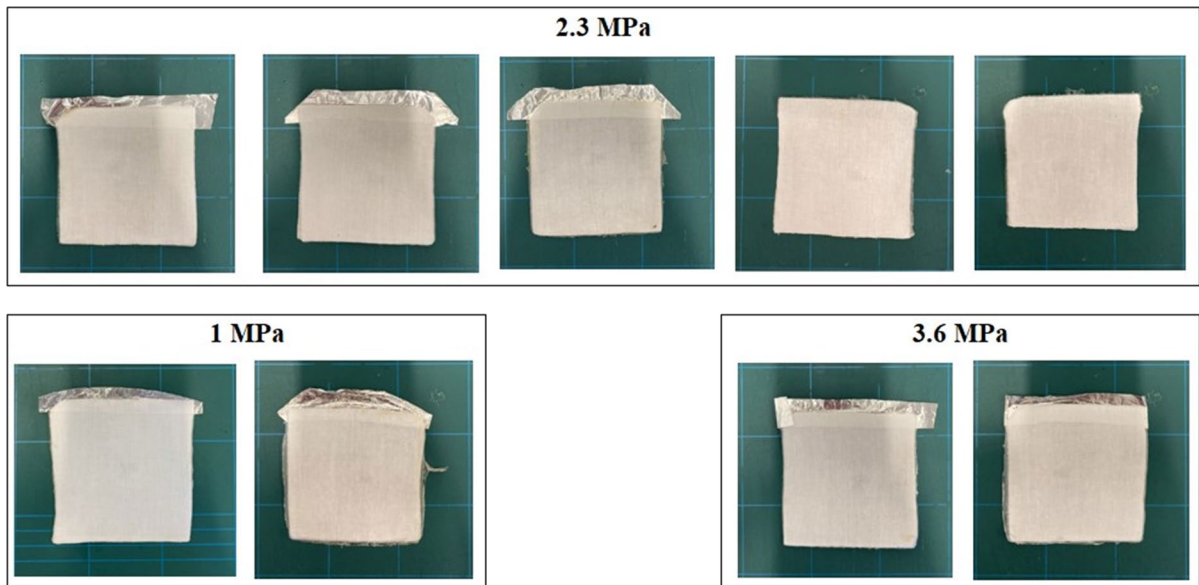
Additional samples were made at pressure settings of 1 and 3.6 MPa respectively to confirm the

insignificance of pressure in the final model, as well as to explore whether this factor affects physical characteristics of the ACCs. For these additional samples, two replicates were made and tested. The COV between the model and the samples made at 1 MPa and 3.6 MPa was 1.7% and 1.1% respectively showing that there is little difference between the variance of the experimental samples and model prediction. The COV between all experimental samples was 0.6%, highlighting the lack of pressure as an influential factor, however, the pressure range used in this study was relatively narrow compared to previous works that have explored this parameter (Adak and Mukhopadhyay 2016; Shibata et al. 2013). It is possible that this pressure range is too narrow to cause any significant change in properties.

#### Characterisation of the optimized ACCs

Table 11 shows additional properties for the samples prepared at the optimum conditions, fixing pressure at 2.3 MPa. Cross-sections from three of these samples are presented in Fig. 14.

Although tensile strength could not be modelled in this work, a value of  $72 \pm 2$  MPa was achieved along with an average peel strength of  $811 \pm 160$  N/m, demonstrating excellent interlaminar strength.

**Fig. 13** Images of ACC samples produced at the identified optimum conditions of 101 °C, and 96.8 min at 2.3 MPa. Additional samples prepared at 1 MPa and 2 MPa are also shown

**Table 11** Measured properties of optimised ACCs prepared at temperature, pressure, and time of 101 °C, 2.3 MPa, and 96.8 min respectively

| Processing conditions                |      |   |      |
|--------------------------------------|------|---|------|
| Temperature (°C)                     | 101  |   |      |
| Pressure (MPa)                       | 2.3  |   |      |
| Time (mins)                          | 96.8 |   |      |
| Properties                           |      |   |      |
| Young's modulus, E (GPa)             | 3.4  | ± | 0.2  |
| Tensile Strength, $\tau$ (MPa)       | 72   | ± | 2    |
| Failure strain (%)                   | 6.4  | ± | 0.2  |
| Peel strength (N/mm)                 | 811  | ± | 160  |
| Thickness (mm)                       | 0.22 | ± | 0.01 |
| Density, $\rho$ (g/cm <sup>3</sup> ) | 1.42 | ± | 0.03 |
| Estimated void content (%)           | 5    | ± | 2    |

Furthermore, a density of  $1.42 \pm 0.03$  g/cm<sup>3</sup> was obtained in these ACCs, exceeding all but one of the density measurements obtained in the original full factorial samples. Sample 9F, prepared at maximum and temperature and time settings had a marginally higher density of  $1.48 \pm 0.01$  g/cm<sup>3</sup>, however, as noted previously this sample showed signs of diminished quality. A density of  $1.42 \pm 0.03$  g/cm<sup>3</sup> is higher than previously reported densities of ACCs prepared from cellulosic fibres such as Lyocell (Adak and Mukhopadhyay 2018; Gindl-Altmutter et al. 2012) and flax (Gindl-Altmutter et al. 2012), for example. Whilst density is not frequently reported in ACCs prepared using textile reinforcement, some comparison can be made to indicate that the density in this work is indeed comparable or higher to that obtained from ACCs made using Lyocell fabric (Adak and Mukhopadhyay 2016), and post-consumer cotton

(Baghaei et al. 2022). It is understood that high density in ACCs indicates a low void content (Korhonen et al. 2019; Uusi-Tarkka et al. 2021) and the void content for these samples can be estimated as  $5 \pm 2\%$ . Excellent consolidation can be seen from the optimised ACCs in, without compromising the balance of matrix and fibre, and this is reflected in the properties obtained. Density, as a powerful factor in driving the mechanical performance of ACCs (Korhonen et al. 2019) is highlighted from these results.

Figure 15 shows the plot of Young's modulus and heat energy used in production, for each of the CCI samples, in order of ascending heat energy. The plot also includes the average Young's modulus and heat energy of the optimized samples (labelled 'Optimized'), showing that there is a good agreement between these, and the center point samples produced at similar processing conditions. Within the boundaries of this response surface design, the center points possess the highest modulus, and have a comparatively lower energy requirement than the samples with similar modulus values.

Sample 10C is the only sample with a Young's modulus close to that obtained from the center points, however with temperature and time settings of 127 °C and 145.3 min respectively, the energy required to produce this sample is significantly higher. Along with tensile strength and density measurements, the optimized samples are desirable across a range of parameters.

It is worth bearing in mind that the inherent variability of natural fibres such as cellulose, as remarked on previously, may inevitably affect the outcomes of different sources of commercially obtained textiles. Whilst the in-lab validation agreed well with the

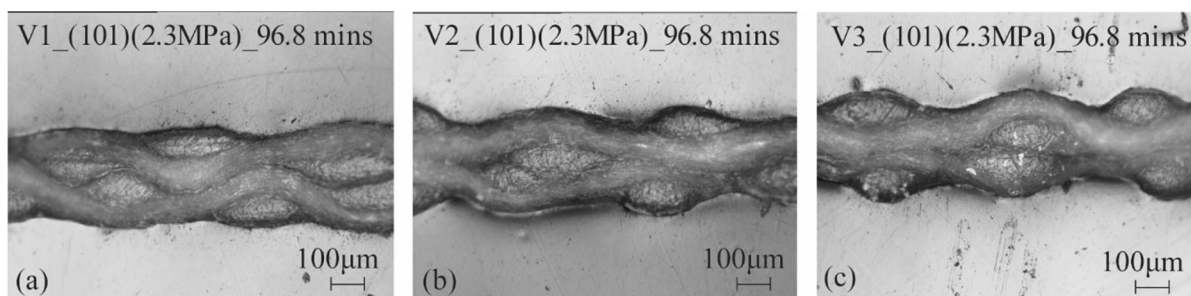


**Fig. 14** Optical microscopy cross-section images of ACC samples prepared at the optimum temperature and time settings as identified from the desirability analysis. Samples are

labelled in the following way, ID(X)(Y)\_Z representing an ACC prepared at a temperature of X °C, a pressure of Y MPa, and a time of Z minutes, prefixed with sample ID

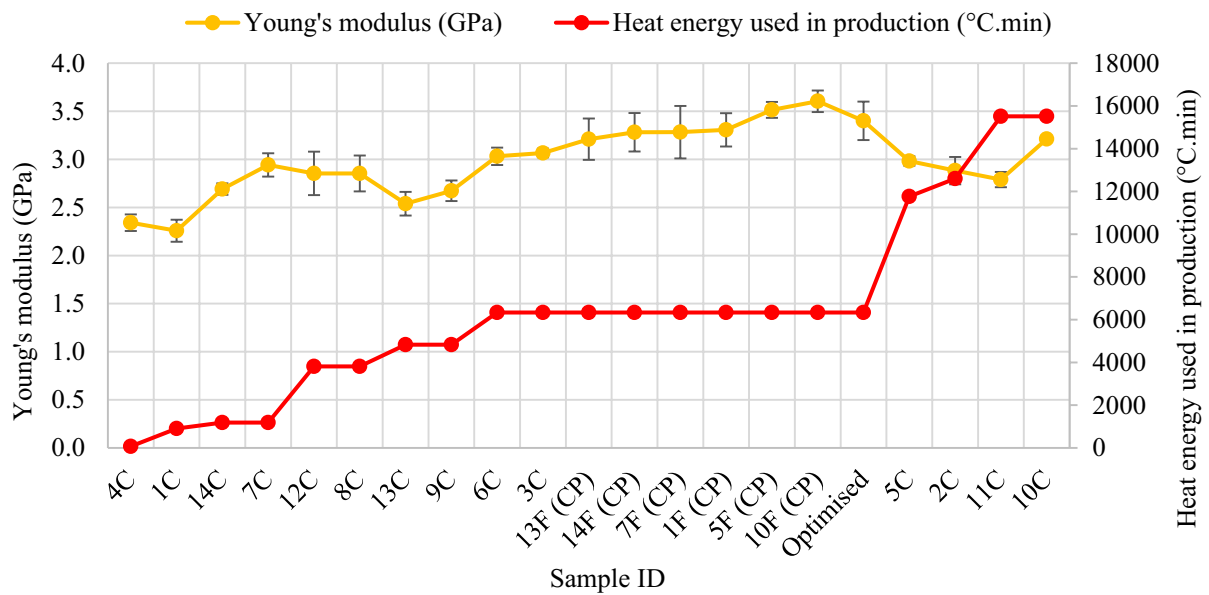


**Fig. 15** Young's modulus and heat energy used in production for each of the samples in the CCI design, plotted in order of ascending heat energy

model prediction for Young's modulus, it is possible that using a different batch of textile may produce different results. The estimation of error calculated from replicate center points, however, does provide an insight into the range of acceptable values for experimental samples to match theory. It would be beneficial to apply DoE methodology to ACC processing using a range of different cellulose sources to explore a wider range of variability and identify whether processing behaviour differs from one source to another.

This work highlights the use of experimental design and optimization in achieving desirable mechanical properties in ACCs and lays the groundwork for future work into the commercialization of ACCs, where identified process conditions can be used as a starting point for process modeling and scale-up. This will allow environmental impacts to be assessed using life cycle analysis (LCA) and techno-economic analysis (TEA). Furthermore, with the insight gained on the applicability of DoE in ACC production, there is potential to incorporate a wider range of responses into the optimization such as impact strength and heat deflection temperature (HDT), for example. Future work will include optimizing ACCs across multiple performance indicators to further expand the potential applications for ACCs.

## Conclusion

The application of statistical DoE was demonstrated as a viable approach to the efficient understanding of ACC preparation. Applied to our previously reported method of combining textile reinforcement and interleaved films, it was possible to model Young's modulus through an inscribed central composite (CCI) design and identify a desirable set of processing conditions that would maximize this property. Validation samples exhibited an average Young's modulus of  $3.4 \pm 0.1$  GPa, when processed at the predicted optimum temperature and time of 101 °C and 96.8 min respectively, agreeing well with the model prediction of 3.3 GPa. Additional mechanical and physical properties were obtained for these samples, providing encouraging insight into the power of statistical DoE to optimise ACC production. Not only was Young's modulus modelled successfully, but the optimised ACCs exhibit an excellent balance of tensile strength, peel strength, Young's modulus, and an important physical property, density. A key driver of this optimisation of mechanical properties would appear to be the elimination of internal voidage, which is a process that takes many hours even at higher temperatures. This an extremely valuable finding, and future

research will concentrate on finding ways to reduce this time to minutes for a viable commercial process.

Furthermore, the insignificance of pressure as a factor in determining Young's modulus was validated by fixing temperature and time at the optimum settings and preparing ACCs at varied pressure settings. The results showed that pressure settings of 1 MPa and 3.6 MPa will yield ACCs with a Young's modulus of  $3.4 \pm 0.1$  GPa and  $3.37 \pm 0.03$  GPa respectively, both in excellent agreement with the model prediction.

This work provides insight into obtaining improved process understanding more efficiently than traditional OFAT methods in the development of ACCs. Furthermore, enhanced insight into process reproducibility has been gained, which supports the future commercialization of such materials. This is an important step in the field of ACCs and the potential applications of statistical modelling. Future work will focus on adapting the process method to explore whether similar optimized properties can be achieved in shorter timescales and applying DoE methodology to different forms of cellulose.

**Acknowledgments** The authors would like to thank Dr. Daniel L. Baker, Experimental Officer in the school of Physics and Astronomy, University of Leeds for experiment training and instruction. The authors would like to thank Professor Tatiana Budtova for her insights into the importance of density in driving mechanical properties of ACCs.

**Author contributions** AV: Conceptualization, Methodology, Investigation, Formal Analysis, Validation, Data curation, Writing- Original draft preparation. MR: Supervision, Conceptualization, Methodology, Data curation, Writing- Reviewing and Editing. KW: Methodology, Data curation, Writing- Reviewing and Editing. PH: Supervision, Conceptualization, Methodology, Data curation, Writing- Reviewing and Editing.

**Funding** This research was supported through a studentship supported by the Engineering and Physical Sciences Research Council (EPSRC) Centre for Doctoral Training in Molecules to Product (EP/SO22473/1). The authors greatly acknowledge their support of this work.

**Data availability** The data associated with this paper are openly available from the University of Leeds Data Repository. <https://doi.org/10.5518/1298>

#### Declarations

**Conflict of interest** The authors have no relevant financial or non-financial interests to disclose.

**Consent for publication** All the authors have given consent for this publication, which includes text, photographs, figures and details within the text to be published in the journal "Cellulose".

**Open Access** This article is licensed under a Creative Commons Attribution 4.0 International License, which permits use, sharing, adaptation, distribution and reproduction in any medium or format, as long as you give appropriate credit to the original author(s) and the source, provide a link to the Creative Commons licence, and indicate if changes were made. The images or other third party material in this article are included in the article's Creative Commons licence, unless indicated otherwise in a credit line to the material. If material is not included in the article's Creative Commons licence and your intended use is not permitted by statutory regulation or exceeds the permitted use, you will need to obtain permission directly from the copyright holder. To view a copy of this licence, visit <http://creativecommons.org/licenses/by/4.0/>.

#### References

- Adak B, Mukhopadhyay S (2016) A comparative study on lyocell-fabric based all-cellulose composite laminates produced by different processes. *Cellulose* 24:835–849. <https://doi.org/10.1007/s10570-016-1149-x>
- Adak B, Mukhopadhyay S (2018) All-cellulose composite laminates with low moisture and water sensitivity. *Polymer* 141:79–85. <https://doi.org/10.1016/j.polymer.2018.02.065>
- Adu C, Zhu C, Jolly M, Richardson RM, Eichhorn SJ (2021) Continuous and sustainable cellulose filaments from ionic liquid dissolved paper sludge nanofibres. *J Clean Prod* 280:124503. <https://doi.org/10.1016/j.jclepro.2020.124503>
- Anderson MJ, Whitcomb PJ (2016) RSM simplified: optimizing processes using response surface methods for design of experiments. CRC Press, Boca Raton. <https://doi.org/10.1201/9781315382326>
- Awais H, Nawab Y, Amjad A, Anjang A, Md Akil H, Zainol Abidin MS (2021) Environmental benign natural fibre reinforced thermoplastic composites: a review. *Compos Part C Open Access* 4:100082. <https://doi.org/10.1016/j.jcomc.2020.100082>
- Azmi H, Haron CHC, Ghani JA, Suhaily M, Yuzairi AR (2017) Machinability Study on Milling Kenaf Fiber Reinforced Plastic Composite Materials using Design of Experiments. In: 3rd International Conference on Science, Technology, and Interdisciplinary Research (IC-STAR). Bandar Lampung, INDONESIA, Iop Publishing Ltd. DOI <https://doi.org/10.1088/1757-899X/344/1/012027>
- Baghaei B, Skrifvars M (2020) All-cellulose composites: a review of recent studies on structure, properties and applications. *Molecules* 25:2836. <https://doi.org/10.3390/molecules25122836>



- Baghaei B, Compieg S, Skrifvars M (2020) Mechanical properties of all-cellulose composites from end-of-life textiles. *J Polym Res* 27:1–9. <https://doi.org/10.1007/s10965-020-02214-1>
- Baghaei B, Johansson B, Skrifvars M, Kadi N (2022) All-cellulose composites properties from pre- and post-consumer denim wastes: comparative study. *J Compos Sci* 6:130. <https://doi.org/10.3390/jcs6050130>
- Baranov A, Sommerhoff F, Duchemin B, Curnow O, Staiger MP (2021) Toward a facile fabrication route for all-cellulose composite laminates via partial dissolution in aqueous tetrabutylphosphonium hydroxide solution. *Compos Part A* 140:106148. <https://doi.org/10.1016/j.compositesa.2020.106148>
- Bawn CSH (1985) Encyclopedia of polymer science and engineering. In: Mark HF, Kroschwitz JI, Bikales N, Overberger CG, Menges G, (ed) Wiley, New York
- Bazboub MB, Taylor M, Baker D, Ries ME, Goswami P (2019) Dry-jet wet electrospinning of native cellulose microfibrers with macroporous structures from ionic liquids. *J Appl Polym Sci* 136:47153. <https://doi.org/10.1002/app.47153>
- Box G, Wilson K (1951) On the experimental attainment of optimum conditions. *J R Stat Soc Series B Stat Methodol* 13:1–38
- Cevheroğlu Çıra S, Dağ A, Karakuş A (2016) Application of response surface methodology and central composite inscribed design for modeling and optimization of marble surface quality. *Adv Mater Sci Eng* 2016:1–13. <https://doi.org/10.1155/2016/2349476>
- Chen F, Sawada D, Hummel M, Sixta H, Budtova T (2020) Unidirectional all-cellulose composites from flax via controlled impregnation with ionic liquid. *Polymers* (basel) 12:1010. <https://doi.org/10.3390/polym12051010>
- de Oliveira LÁ, Santos JcD, Panzera TH, Freire RTS, Vieira LMG, Rubio JCC (2018) Investigations on short coir fibre-reinforced composites via full factorial design. *Polym Polym Compos* 26:391–399. <https://doi.org/10.1177/0967391118806144>
- Derringer G, Suich R (1980) Simultaneous optimization of several response variables. *J Qual Technol* 12:214–219. <https://doi.org/10.1080/00224065.1980.11980968>
- Dozie KCN, Nwanya JC (2020) Optimal prediction variance capabilities of inscribed central composite designs. *Asian J Probab Stat* 8:1–8. <https://doi.org/10.9734/ajpas/2020/v8i130194>
- Duchemin BJC, Mathew AP, Oksman K (2009) All-cellulose composites by partial dissolution in the ionic liquid 1-butyl-3-methylimidazolium chloride. *Compos Part A* 40:2031–2037. <https://doi.org/10.1016/j.compositesa.2009.09.013>
- Errero A, Jones B, Li W, Nachtsheim CJ (2017) Using definitive screening designs to identify active first-and second-order factor effects. *J Qual Technol* 49:244–264. <https://doi.org/10.1080/00224065.2017.11917993>
- Favre H, Chaves Neto A (2021) An application of definitive screening designs (DSDs) to a food product optimization and adaptations to jones & nachtsheim methodology for fitting DSD models. *Food Qual Prefer* 88:104106. <https://doi.org/10.1016/j.foodqual.2020.104106>
- Filho SLMR, Garcia CT, Donadon MV, Scarpa F, Panzera TH (2022) The impact behaviour of hybrid fibre-particle composites based on a full factorial design. *Mater Today Commun* 31:103459. <https://doi.org/10.1016/j.mtcomm.2022.103459>
- Fukuda IM, Pinto CFF, Moreira CdS, Saviano AM, Lourenço FR (2018) Design of experiments (DoE) applied to pharmaceutical and analytical quality by design (QbD). *Braz J Pharm Sci*. <https://doi.org/10.1590/s2175-97902018000001006>
- Garnier C, Mistou S, Pantalé O (2010) Influence of process and material parameters on impact response in composite structure: methodology using design of experiments. *Key Eng* 446:83–90. <https://doi.org/10.4028/www.scientific.net/KEM.446.83>
- Ghandi K (2014) A review of ionic liquids, their limits and applications. *Green Sustain Chem* 04:44–53. <https://doi.org/10.4236/gsc.2014.41008>
- Gindl W, Keckes J (2005) All-cellulose nanocomposite. *Polymer* 46:10221–10225. <https://doi.org/10.1016/j.polymer.2005.08.040>
- Gindl-Altmatter W, Keckes J, Plackner J, Liebner F, Englund K, Laborie M-P (2012) All-cellulose composites prepared from flax and lyocell fibres compared to epoxy-matrix composites. *Compos Sci Technol* 72:1304–1309. <https://doi.org/10.1016/j.compscitech.2012.05.011>
- Gujral G, Kapoor D, Jaimini M (2018) An updated review on design of experiment (Doe) in pharmaceuticals. *J Drug Delivery Ther* 8:147–152. <https://doi.org/10.22270/jddt.v8i3.1713>
- Gunaraj V, Murugan N (1999) Application of response surface methodology for predicting weld bead quality in submerged arc welding of pipes. *J Mater Process Technol* 88:266–275. [https://doi.org/10.1016/S0924-0136\(98\)00405-1](https://doi.org/10.1016/S0924-0136(98)00405-1)
- Halley P (2020) Sustainable plastics inspired by nature. *Physics* 13:126. <https://doi.org/10.1103/Physics.13.126>
- Harmsen J (2014) Novel sustainable industrial processes: from idea to commercial scale implementation. *Green Process Synth* 3:189–193. <https://doi.org/10.1515/gps-2013-0102>
- Hauru LK, Hummel M, King AW, Kilpelainen I, Sixta H (2012) Role of solvent parameters in the regeneration of cellulose from ionic liquid solutions. *Biomacromol* 13:2896–2905. <https://doi.org/10.1021/bm300912y>
- Haverhals LM, Sulpizio HM, Fayos ZA, Trulove MA, Reichert WM, Foley MP, De Long HC, Trulove PC (2011) Process variables that control natural fiber welding: time, temperature, and amount of ionic liquid. *Cellulose* 19:13–22. <https://doi.org/10.1007/s10570-011-9605-0>
- Hawkins JE, Liang Y, Ries ME, Hine PJ (2021) Time temperature superposition of the dissolution of cellulose fibres by the ionic liquid 1-ethyl-3-methylimidazolium acetate with cosolvent dimethyl sulfoxide. *Carbohydr Polym Technol Appl* 2:100021. <https://doi.org/10.1016/j.carpta.2020.100021>
- Hine PJ, Ries ME (2020) Composite materials. Patent number: WO2020016583, International Patent (GB, Europe, USA, Japan). <https://patentscope.wipo.int/search/en/detail.jsf?docId=WO2020016583>
- Huber T, Bickerton S, Mussig J, Pang S, Staiger MP (2012a) Solvent infusion processing of all-cellulose composite materials. *Carbohydr Polym* 90:730–733. <https://doi.org/10.1016/j.carbpol.2012.05.047>

- Huber T, Pang S, Staiger MP (2012b) All-cellulose composite laminates. *Compos Part A Appl Sci Manuf* 43(10):1738–1745. <https://doi.org/10.1016/j.compositesa.2012.04.017>
- Hull D, Clyne TW (1996) Fabrication. In: Hull D, Clyne TW (eds) *An introduction to composite materials*. Cambridge University Press, Cambridge. <https://doi.org/10.1017/CBO9781139170130.013>
- Jankovic A, Chaudhary G, Goia F (2021) Designing the design of experiments (DOE)—an investigation on the influence of different factorial designs on the characterization of complex systems. *Energy Build* 250:111298. <https://doi.org/10.1016/j.enbuild.2021.111298>
- Johnson DJ (2003) A framework for reducing manufacturing throughput time. *J Manuf Syst* 22:283–298. [https://doi.org/10.1016/S0278-6125\(03\)80009-2](https://doi.org/10.1016/S0278-6125(03)80009-2)
- Jones B, Nachtsheim CJ (2011) A class of three-level designs for definitive screening in the presence of second-order effects. *J Qual Technol* 43:1–15. <https://doi.org/10.1080/00224065.2011.11917841>
- Jun Z, Xiang-Ming W, Jian-Min C, Kai Z (2008) Optimization of processing variables in wood-rubber composite panel manufacturing technology. *Bioresour Technol* 99:2384–2391. <https://doi.org/10.1016/j.biortech.2007.05.031>
- Kandar MIM, Akil HM (2016) Application of design of experiment (DoE) for parameters optimization in compression moulding for flax reinforced biocomposites. *Proc Chem* 19:433–440. <https://doi.org/10.1016/j.proche.2016.03.035>
- Kidwai NH, Singh H, Chatterjee A (2020) All-cellulose composite from cotton fabric and cellulose solution. *Cellul Chem Technol* 54:757–764
- Klemm D, Heublein B, Fink HP, Bohn A (2005) Cellulose: fascinating biopolymer and sustainable raw material. *Angew Chem Int Ed Engl* 44:3358–3393. <https://doi.org/10.1002/anie.200460587>
- Korhonen O, Sawada D, Budtova T (2019) All-cellulose composites via short-fiber dispersion approach using NaOH-water solvent. *Cellulose* 26:4881–4893. <https://doi.org/10.1007/s10570-019-02422-z>
- Ku H, Wang H, Pattarachaiyakoop N, Trada M (2011) A review on the tensile properties of natural fiber reinforced polymer composites. *Compos Part B Eng* 42:856–873. <https://doi.org/10.1016/j.compositesb.2011.01.010>
- Kumar BS, Balachandrar S (2014) A study on the influence of hot press forming process parameters on flexural property of glass/pp based thermoplastic composites using box-behken experimental design. *ISRN Mater Sci* 2014:1–6. <https://doi.org/10.1155/2014/624045>
- Lee R (2019) Statistical design of experiments for screening and optimization. *Chem Ing Tech* 91:191–200. <https://doi.org/10.1002/cite.201800100>
- Lee BCY, Mahtab MS, Neo TH, Farooqi IH, Khursheed A (2022) A comprehensive review of design of experiment (DOE) for water and wastewater treatment application-key concepts, methodology and contextualized application. *J Water Process Eng* 47:102673. <https://doi.org/10.1016/j.jwpe.2022.102673>
- Liang Y, Hawkins JE, Ries ME, Hine PJ (2020) Dissolution of cotton by 1-ethyl-3-methylimidazolium acetate studied with time-temperature superposition for three different fibre arrangements. *Cellulose* 28:715–727. <https://doi.org/10.1007/s10570-020-03576-x>
- Liao W, Liu Y, Wen Z, Frear C, Chen S (2007) Studying the effects of reaction conditions on components of dairy manure and cellulose accumulation using dilute acid treatment. *Bioresour Technol* 98:1992–1999. <https://doi.org/10.1016/j.biortech.2006.08.021>
- Mat Salleh M, Magniez K, Pang S, Dormanns JW, Staiger MP (2017) Parametric optimization of the processing of all-cellulose composite laminae. *Adv Manuf Polym Compos Sci* 3:73–79. <https://doi.org/10.1080/20550340.2017.1324351>
- Matthews FL, Rawlings RD (1999) *Composite materials: engineering and science*. Chapman & Hall, London
- McKillup S (2011) *Statistics explained: an introductory guide for life scientists*. Cambridge University Press, Cambridge
- Misra M, Vivekanandhan S, Mohanty AK, Denault J (2011) 4.10 Nanotechnologies for agricultural bioproducts. In: Moo-Young M (ed) *Comprehensive biotechnology*, 3rd edn. Pergamon, Oxford
- Mohammed A, Rivers A, Stuckey DC, Ward K (2020) Alginate extraction from sargassum seaweed in the caribbean region: optimization using response surface methodology. *Carbohydr Polym* 245:116419. <https://doi.org/10.1016/j.carbpol.2020.116419>
- Mohammed A, Gaduan A, Chaitram P, Pooran A, Lee K-Y, Ward K (2023) Sargassum inspired, optimized calcium alginate bioplastic composites for food packaging. *Food Hydrocoll*. <https://doi.org/10.1016/j.foodhyd.2022.108192>
- Montgomery DC (2017) *Design and analysis of experiments*. Wiley, New York
- Mwaikambo LY, Ansell MP (2001) The determination of porosity and cellulose content of plant fibers by density methods. *J Mater Sci Lett* 20:2095–2096. <https://doi.org/10.1023/A:1013703809964>
- Nagavally RR (2017) Composite materials-history, types, fabrication techniques, advantages, and applications. *Int J Mech Prod Eng* 5:82–87
- Nishino T, Arimoto N (2007) All-cellulose composite prepared by selective dissolving of fiber surface. *Biomacromol* 8:2712–2716. <https://doi.org/10.1021/bm0703416>
- Nishino T, Matsuda I, Hirao K (2004) All-cellulose composite. *Macromolecules* 37:7683–7687. <https://doi.org/10.1021/ma049300h>
- Noordin MY, Venkatesh VC, Sharif S, Elting S, Abdullah A (2004) Application of response surface methodology in describing the performance of coated carbide tools when turning AISI 1045 steel. *J Mater Process Technol* 145:46–58. [https://doi.org/10.1016/S0924-0136\(03\)00861-6](https://doi.org/10.1016/S0924-0136(03)00861-6)
- Odalanowska M, Skrzypczak A, Borysiak S (2021) Innovative ionic liquids as functional agent for wood-polymer composites. *Cellulose* 28:10589–10608. <https://doi.org/10.1007/s10570-021-04190-1>
- Oliveira LÁ, Santos JC, Panzera TH, Freire RTS, Vieira LMG, Scarpa F (2018) Evaluation of hybrid-short-coir-fibre-reinforced composites via full factorial design. *Compos Struct* 202:313–323. <https://doi.org/10.1016/j.compstruct.2018.01.088>
- Oneil MJ (2013) *The merck index - an encyclopedia of chemicals, drugs, and biologicals* royal society of chemistry. RSC Publishing, Cambridge



- Osborne J (2010) Improving your data transformations: applying the box-cox transformation. *Pract Assess Res Eval* 15:12. <https://doi.org/10.7275/qbpc-gk17>
- Owen MR, Luscombe C, Lai L-W, Godbert S, Crookes DL, Emiabata-Smith D (2001) Efficiency by design: optimisation in process research. *Org Process Res Dev* 5:308–323. <https://doi.org/10.1021/op000024q>
- Pinkert A, Kenneth M (2008) Ionic liquids and their interaction with cellulose. *Chem Rev* 109:6712–6728. <https://doi.org/10.1021/cr9001947>
- Romli FI, Alias AN, Rafie ASM, Majid DLAA (2012) Factorial study on the tensile strength of a coir fiber-reinforced epoxy composite. *AASRI Proc* 3:242–247. <https://doi.org/10.1016/j.aasri.2012.11.040>
- Rosenboom JG, Langer R, Traverso G (2022a) Bioplastics for a circular economy. *Nat Rev Mater*. <https://doi.org/10.1038/s41578-021-00407-8>
- Sescousse R, Le KA, Ries ME, Budtova T (2010) Viscosity of cellulose-imidazolium-based ionic liquid solutions. *J Phys Chem* 114:7222–7228. <https://doi.org/10.1021/jp1024203>
- Shibata M, Teramoto N, Nakamura T, Saitoh Y (2013) All-cellulose and all-wood composites by partial dissolution of cotton fabric and wood in ionic liquid. *Carbohydr Polym* 98:1532–1539. <https://doi.org/10.1016/j.carbpol.2013.07.062>
- Soykeabkaew N, Nishino T, Peijs T (2009) All-cellulose composites of regenerated cellulose fibres by surface selective dissolution. *Compos Part A* 40:321–328. <https://doi.org/10.1016/j.compositesa.2008.10.021>
- Spörl JM, Batti F, Vocht M-P, Raab R, Müller A, Hermanutz F, Buchmeiser MR (2018) Ionic liquid approach toward manufacture and full recycling of all-cellulose composites. *Macromol Mater Eng* 303:1700335. <https://doi.org/10.1002/mame.201700335>
- Swatloski RP (2002) Dissolution of cellulose with ionic liquids. *Am Chem Soc* 4974:4974–4975. <https://doi.org/10.1021/ja025790m>
- Tholibon D, Sulong AB, Muhamad N, Farhani N, Tharazi I, Md Radzi MKF (2017b) Optimization of hot pressing process for unidirectional kenaf polypropylene composites by full factorial design. *J Mech Eng* S13:23–35
- Todor M-P, Kiss I, Cioata VG (2021) Development of fabric-reinforced polymer matrix composites using bio-based components from post-consumer textile waste. *Mater Today Proc*. <https://doi.org/10.1016/j.matpr.2020.11.927>
- Uusi-Tarkka E-K, Skrifvars M, Haapala A (2021) Fabricating sustainable all-cellulose composites. *Appl Sci*. <https://doi.org/10.3390/app112110069>
- Vanaja K, Shobha Rani RH (2008) Design of experiments: concept and applications of Plackett Burman design. *Clin Res Regul Aff* 24:1–23. <https://doi.org/10.1080/10601330701220520>
- Vanaret C, Seufert P, Schwientek J, Karpov G, Ryzhakov G, Oseledets I, Aspiron N, Bortz M (2021) Two-phase approaches to optimal model-based design of experiments: how many experiments and which ones? *Comput Chem Eng*. <https://doi.org/10.1016/j.compchemeng.2020.107218>
- Vicente G, Coteron A, Martinez M, Aracil J (1998) Application of the factorial design of experiments and response surface methodology to optimize biodiesel production. *Ind Crops Prod* 8:29–35. [https://doi.org/10.1016/S0926-6690\(97\)10003-6](https://doi.org/10.1016/S0926-6690(97)10003-6)
- Victoria A, Edward Ries M, John Hine P (2022b) Use of interleaved films to enhance the properties of all-cellulose composites. *Compos Part A*. <https://doi.org/10.1016/j.compositesa.2022.107062>
- Wang J, Wang L, Gardner DJ, Shaler SM, Cai Z (2021) Towards a cellulose-based society: opportunities and challenges. *Cellulose*. <https://doi.org/10.1007/s10570-021-03771-4>
- Weissman SA, Anderson NG (2014) Design of experiments (DoE) and process optimization. A review of recent publications. *Org Process Res Dev* 19:1605–1633. <https://doi.org/10.1021/op500169m>
- Zhao Q, Yam RCM, Zhang B, Yang Y, Cheng X, Li RKY (2008) Novel all-cellulose ecomposites prepared in ionic liquids. *Cellulose* 16:217–226. <https://doi.org/10.1007/s10570-008-9251-3>
- Zhou Y-D, Xu H (2017) Composite designs based on orthogonal arrays and definitive screening designs. *J Am Stat Assoc* 112:1675–1683. <https://doi.org/10.1080/01621459.2016.1228535>

**Publisher's Note** Springer Nature remains neutral with regard to jurisdictional claims in published maps and institutional affiliations.